



Evaluation of vertical coordinate and vertical mixing algorithms in the HYbrid-Coordinate Ocean Model (HYCOM)

George R. Halliwell

MPO/RSMAS, University of Miami, 4600 Rickenbacker Causeway, Miami, FL 33149, USA

Received 31 July 2002; received in revised form 2 July 2003; accepted 7 October 2003

Available online 4 December 2003

Abstract

Vertical coordinate and vertical mixing algorithms included in the HYbrid Coordinate Ocean Model (HYCOM) are evaluated in low-resolution climatological simulations of the Atlantic Ocean. The hybrid vertical coordinates are isopycnic in the deep ocean interior, but smoothly transition to level (pressure) coordinates near the ocean surface, to sigma coordinates in shallow water regions, and back again to level coordinates in very shallow water. By comparing simulations to climatology, the best model performance is realized using hybrid coordinates in conjunction with one of the three available differential vertical mixing models: the nonlocal K-Profile Parameterization, the NASA GISS level 2 turbulence closure, and the Mellor–Yamada level 2.5 turbulence closure. Good performance is also achieved using the quasi-slab Price–Weller–Pinkel dynamical instability model. Differences among these simulations are too small relative to other errors and biases to identify the “best” vertical mixing model for low-resolution climate simulations. Model performance deteriorates slightly when the Kraus–Turner slab mixed layer model is used with hybrid coordinates. This deterioration is smallest when solar radiation penetrates beneath the mixed layer and when shear instability mixing is included. A simulation performed using isopycnic coordinates to emulate the Miami Isopycnic Coordinate Ocean Model (MICOM), which uses Kraus–Turner mixing without penetrating shortwave radiation and shear instability mixing, demonstrates that the advantages of switching from isopycnic to hybrid coordinates and including more sophisticated turbulence closures outweigh the negative numerical effects of maintaining hybrid vertical coordinates.

© 2003 Elsevier Ltd. All rights reserved.

E-mail address: ghalliwell@rsmas.miami.edu (G.R. Halliwell).

1. Introduction

The HYbrid Coordinate Ocean Model (HYCOM) is a primitive equation ocean general circulation model that evolved from the Miami Isopycnic-Coordinate Ocean Model (MICOM). MICOM has become one of the primary ocean models in use today, having been subjected to validation studies (e.g. Chassignet et al., 1996; Roberts et al., 1996) and used in numerous ocean climate studies (e.g., New and Bleck, 1995; New et al., 1995; Hu, 1996, 1997; Halliwell, 1997, 1998; Bleck, 1998; Paiva et al., 2000). MICOM vertical coordinates are isopycnic except for model layer one, which is a non-isopycnic slab mixed layer.

Model comparisons run in Europe (Dynamics of North Atlantic Models, or DYNAMO; Willebrand et al., 2001) and in the US (Data Assimilation and Model Evaluation Experiment, or DAMEE; Chassignet et al., 2000) demonstrate that interior water mass distribution and thermohaline circulation patterns are very sensitive to processes that are not reproduced with equal fidelity in models with different vertical coordinate discretizations. Advantages of isopycnic-coordinate models such as MICOM include: (1) the absence of numerically induced diapycnal mixing and (2) the ability to efficiently resolve baroclinic structure with relatively few vertical coordinates. Disadvantages include: (1) providing inadequate vertical resolution in regions with weak stratification, including the surface mixed layer; and (2) being suboptimum in the coastal ocean and shallow seas where topographic changes are large and bottom boundary layer dynamics is usually important. All MICOM isopycnic layers with reference densities smaller than the mixed layer density collapse to zero thickness at the mixed layer base (MLB). Only slab mixed layer models can be used, and MICOM is equipped with a Kraus–Turner model (Turner and Kraus, 1967; Niiler and Kraus, 1977) that employs the modified TKE parameterization of Gaspar (1988). The HYCOM hybrid coordinate algorithm was developed to overcome these MICOM limitations by placing different vertical coordinates types in those regions where they are quasi-optimum, and thus permitting the use of more sophisticated turbulence closures.

The parameterization of vertical mixing is a limiting factor in all types of ocean models. OGCM studies are typically conducted using one set of parameterizations to govern vertical mixing, including the strong mixing in the near surface mixed layer, the relatively weak mixing in the ocean interior, and in some cases the enhanced mixing of the bottom boundary layer, without documenting the sensitivity of scientific results to this choice. For example, the Kraus–Turner mixed layer model supplemented by the McDougall and Dewar (1998) interior diapycnal-mixing model is the only vertical mixing option presently available in MICOM. At present, no single vertical mixing model exists that is clearly the optimum choice to use in ocean models. The alternate strategy employed in HYCOM is to equip it with a selection of state-of-the-art vertical mixing models to allow the user to: (1) determine the sensitivity of scientific conclusions to vertical mixing choice and (2) determine the best vertical mixing model for the particular ocean environment being simulated.

The initial hybrid coordinate development effort involved implementing the transition between an isopycnic coordinate ocean interior and a level (p) coordinate domain near the ocean surface. Bleck (2002) describes the development of this algorithm and validates its performance in a low-resolution global simulation that used a simple Kraus–Turner mixed layer model. Since then, the hybrid coordinate algorithm has evolved substantially. The coordinates remain isopycnic in the open stratified ocean, but smoothly transition to level (p) coordinates in weakly-stratified regions

such as the surface mixed layer, to terrain-following sigma coordinate in shallow water regions, then back to p coordinates in very shallow water to prevent layers from becoming too thin. It is possible to run the model as a purely p -coordinate model, as a purely sigma-coordinate model, and as an isopycnic-coordinate model capped by a single slab mixed layer to emulate MICOM, with the latter configuration referred to as MICOM mode. Model performance for scenarios excluding pure sigma coordinates has been evaluated in HYCOM experiments conducted within the WOCE Community Modelling Experiment domain (Chassignet et al., 2003). The present study emphasizes the standard hybrid coordinate configuration designed to preserve the advantage of isopycnic coordinates throughout as much of the water column as possible beneath the surface mixed layer.

The present analysis builds on the study of Bleck (2002) by documenting subsequent development of the hybrid vertical coordinate algorithm and by documenting the several vertical mixing submodels that have since been included. These submodels are evaluated using low-resolution climatological simulations of the Atlantic Ocean. Given the low resolution, the coastal transition to sigma coordinates is not considered. Analysis of that transition along with the validation of other new and improved capabilities included in the latest release of HYCOM, such as advanced nesting capability, will be performed in future studies. Several hybrid coordinate experiments are performed to evaluate all vertical mixing choices that have been implemented. Model sensitivity to vertical coordinate choice is evaluated by comparing a MICOM mode simulation to these hybrid experiments. By comparing all simulations to climatology, it is possible to demonstrate improvements resulting from the use of hybrid vertical coordinates in conjunction with improved vertical mixing algorithms. However, errors due to other factors are large enough to make it impossible to select the best vertical mixing choice for these low-resolution climate simulations.

The full suite of model capabilities is presented in the HYCOM Users Manual (Bleck et al., 2002). This Manual, along with other model information, publications, and ongoing research summaries, is available on the internet at <http://hycom.rsmas.miami.edu>.

2. Recent HYCOM algorithm development

2.1. Overview

The development of hybrid coordinate modelling and the philosophical rationale supporting it are discussed in Bleck (2002) and Bleck and Benjamin (1993). The fundamental HYCOM equations are presented in Bleck (2002), as is a description of the simple energy loan ice model embedded in HYCOM. The present paper concentrates almost entirely on model development that has occurred since Bleck (2002), emphasizing changes to the hybrid coordinate adjustment algorithm, the new vertical mixing algorithms, and other related modifications. Only general summaries are presented here. Technical details of the implementation of these algorithms have been included in the HYCOM Users Manual (Bleck et al., 2002, available at <http://hycom.rsmas.miami.edu>). HYCOM variables are stored on the Arakawa C grid, with momentum components carried at u and v grid points and thermodynamical variables plus tracers stored at

pressure (p) grid points. All one-dimensional submodels embedded in HYCOM are designed to work on this staggered grid.

The full set of vertical mixing options embedded in HYCOM is summarized in Table 1. There are seven primary vertical mixing algorithms, of which three are “continuous” differential models and four are bulk (slab) models. The three differential models are the nonlocal K-Profile Parameterization (KPP; Large et al., 1994], the NASA Goddard Institute for Space Studies level 2 turbulence closure (GISS; Canuto et al., 2001, 2002), and the Mellor–Yamada level 2.5 turbulence closure (MY; Mellor and Yamada, 1982). These models govern vertical mixing throughout the water column. The bulk models include the dynamical instability model of Price et al. (1986) (PWP) and three versions of the Kraus–Turner model. Two of these versions are designed to work with hybrid vertical coordinates: an accurate (but relatively inefficient) version (KTA) along with a simplified (less accurate but more efficient) version (KTB). The KTB model was used in the global simulation of Bleck (2002). A third version of the KT model (KTC) obtained from MICOM version 2.8 is used when the model is run with isopycnic vertical coordinates (MICOM mode). For the slab mixed layer models, three supplemental interior diapycnal mixing algorithms are included to mix the interior ocean. Two of these are designed to work with hybrid vertical coordinates: an explicit (MICOM-like) and an implicit (KPP-like) algorithm. The third is

Table 1
Vertical mixing options embedded in HYCOM

Mixing model	Description	Supplemental interior diapycnal mixing algorithms	Additional choices
KPP (K-Profile Parameterization)	Nonlocal differential model	Not required	
GISS (NASA Goddard Institute for Space Studies)	Local differential Reynolds stress model; level 2 turbulence closure	Not required	
MY (Mellor–Yamada)	Local differential Reynolds stress model; level 2.5 turbulence closure	Not required	
PWP (Price–Weller–Pinkel)	Slab m. l.; static instability; bulk and gradient Richardson number instabilities	Explicit (MICOM-like) for hybrid coordinates	
KTA (Full Kraus–Turner for hybrid coordinates)	Slab m. l., vertically integrated TKE balance	1. Explicit (MICOM-like) for hybrid coordinates 2. Implicit (KPP-like) for hybrid coordinates	Penetrating short-wave radiation (yes or no)
KTB (Simplified Kraus–Turner for hybrid coordinates)	Slab m. l., vertically integrated TKE balance	1. Explicit (MICOM-like) for hybrid coordinates 2. Implicit (KPP-like) for hybrid coordinates	
KTC [Kraus–Turner for isopycnic coordinates (MICOM mode)]	Slab m. l., vertically integrated TKE balance (from MICOM 2.8)	Explicit for isopycnic coordinates (from MICOM 2.8)	

the explicit algorithm extracted from MICOM 2.8 and used when the model is run in MICOM mode.

2.2. Hybrid coordinate grid generator

Technical details of the “grid generator” that maintains the hybrid vertical coordinates are presented in the HYCOM Users Manual (Bleck et al., 2002). The following discussion emphasizes changes relevant to the present study made since the analysis of Bleck (2002). Non-relevant changes such as the coastal sigma coordinate transition are not discussed.

The grid generator is the final algorithm executed during each model time step. It first attempts to restore the density of a given layer to the isopycnic reference density if necessary. If a layer is less dense than its isopycnic reference density, the model attempts to move the interface at the bottom downward so that the flux of denser water across this interface restores isopycnic density. If the layer is too dense, the model attempts to move the upper interface upward. To enforce minimum thickness, a constant minimum thickness δ_k is specified separately for each model layer k . As a result, layers near the surface with densities exceeding their reference values cannot have isopycnic conditions restored. The algorithm attempts to raise the interfaces above each layer to entrain lighter water, but is blocked by minimum thickness enforcement using a “cushion” function (Bleck, 2002) that produces a smooth transition from the isopycnic to the p domain. The current form of this function is presented in the HYCOM Users Manual (Bleck et al., 2002). The trick to establishing a p -coordinate domain near the surface year round is to initialize the uppermost layers with reference densities smaller than values found anywhere in the model domain. In the latest HYCOM release, model layer 1 is always maintained at a constant thickness of δ_1 . The number of level p coordinates (constant thickness layers) below layer 1 then depends in part on the number of layers initialized with these small reference densities. The minimum thickness constraint is not enforced at the bottom in the open ocean, permitting model layers to collapse to zero thickness there as in MICOM.

If small values of δ_k are specified, a thin p domain will exist near the surface that provides high vertical resolution in the thin summer mixed layer but poor resolution in most of the deep winter mixed layer. If large values are specified, a thick p domain will exist that provides relatively even resolution throughout the deep winter mixed layer, but that extends far below the thin summer mixed layer. In the present analysis, an intermediate constant value of δ_k (10 m) is chosen to avoid both of these extremes. Properties of the chosen grid during summer and winter are illustrated in Fig. 1.

Specifying large δ_k has the undesirable effect of inhibiting the formation of sharp pycnoclines in the isopycnic ocean interior. For this reason, code was developed at the Naval Research Laboratory (A.J. Wallcraft, personal communication) to override the globally specified minimum thicknesses δ_k for all isopycnic layers k beneath the nearsurface p coordinate domain. It is replaced by a new minimum thickness δ_{\min} , which is set to two meters in the present study. A linear “cushion function” enforces a smooth transition between layers governed by minimum thickness δ_k and those governed by δ_{\min} .

Several other modifications have been made since Bleck (2002) to improve performance. In general, cabbelling prevents perfect restoration of isopycnic conditions when T and S are entrained across the relocated interface into the receiving layer. During HYCOM development, cabbelling

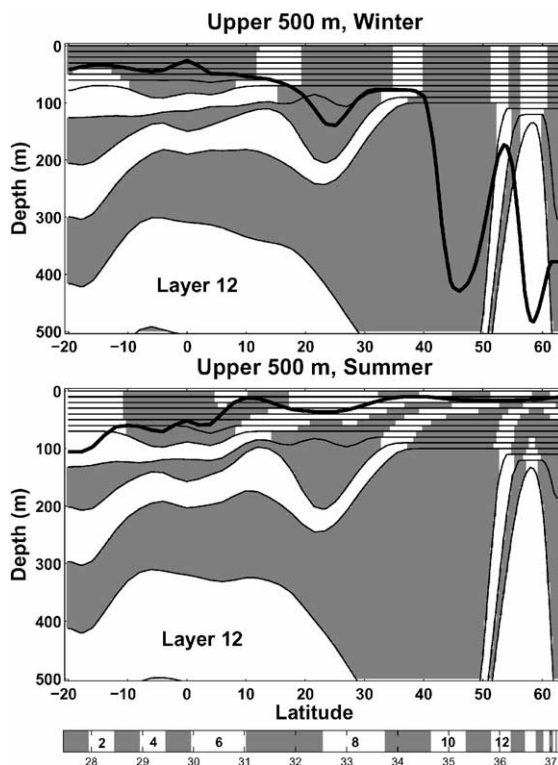


Fig. 1. Cross-section of model density (σ_2) along 29W during winter (top) and summer (bottom) over the upper 500 m from a simulation run using KPP mixing. The density range in the bottom bar is divided into alternate white and gray bands, with each band centered on the reference density of a model layer. Even-number model layers are white, and some of these numbers are marked inside the bar. The alternating white and gray bands follow model layers only in the isopycnic domain. The thick solid line represents the diagnosed mixed layer base.

resulting from both vertical coordinate adjustment and horizontal T , S advection and diffusion caused excessive interface relocation in limited regions such as beneath the Mediterranean salt tongue. The nonlinear equation of state can, for certain T , S profiles, produce either insignificant density changes or density changes of the wrong sign within a model layer when the grid generator relocates an interface. For this reason, HYCOM now gives the user the option of specifying any two of the three thermodynamical variables T , S , ρ to be horizontally advected and diffused, and also to be fluxed across relocated interfaces, with the third being diagnosed by the equation of state. If T , ρ or ρ , S are selected, then horizontal advection and diffusion both maintain isopycnic conditions in the interior while an accurate restoration of isopycnic conditions by the grid generator is possible unless overridden by the minimum thickness specification. The tradeoff is that either temperature or salinity is no longer conserved.

To limit the negative influence of cabling on the grid generator, two modifications were made: first, vertical interfaces are not relocated wherever the nonlinear equation of state produces density changes of the wrong sign or does not permit isopycnic density restoration without excessive interface relocation. Second, an iterative algorithm was added that allows the resulting

layer density to converge to the target isopycnic density. With these modifications, T and S are chosen here to be the variables fluxed across relocated interfaces, and also horizontally advected and diffused, without encountering excessive vertical coordinate relocation. Advantages to choosing T and S are addressed in Section 4.3.4.

For compatibility with the KTA mixed layer model, an unmixing algorithm has been added to re-stratify the water column within the layer containing the MLB (see Section 2.4.5). Code has also been included to break down interior blocking layers that arise when a model interface cannot be moved upward or downward to restore isopycnic conditions within a given layer because the layer above or below is too thin. The donor cell scheme used to remap model layer variables from the old vertical grid onto the relocated grid has been modified so that the final values of layer variables do not depend on whether the remapping algorithm is executed upward or downward. (The alternating donor cell and unmixing algorithm tested by Bleck (2002) is not implemented here or in the current HYCOM release). Donor-cell schemes are known to produce numerically induced diffusion. For this reason, the re-mapping scheme was modified at the Naval Research Laboratory (A.J. Wallcraft, personal communication) to use the higher-order PLM algorithm within the nearsurface non-isopycnic domain. The PLM algorithm is only executed there because the distance that interfaces are relocated, and thus the magnitude of numerical diffusion, is relatively large. In the isopycnic interior, the original remapping algorithm is retained in part because the PLM algorithm has the undesirable effect of changing layer variables when fluid is only detrained from a given layer.

After adjusting interface depths, thermodynamical variables, and scalar tracers at p grid points, momentum components are adjusted by horizontally interpolating the new interface depths to u and v grid points, and then remapping u and v on their native grids.

2.3. *Surface and bottom fluxes*

The bulk formula parameterization of Kara et al. (2000b) for calculating evaporation and air-sea heat fluxes has been included in HYCOM and used in the present study. In addition to surface flux forcing, it is also possible to relax either or both surface T and S to climatology over a user-specified thickness. For some vertical mixing choices, shortwave radiation can be distributed over model layers using the two-component (red and blue) exponential decay model of Jerlov (1976). In the full Kraus–Turner model (KTA), penetrating shortwave radiation is an option. If it is invoked, the shortwave radiation that is not absorbed within the mixed layer is distributed over model layers beneath the MLB. If it is not invoked, or if the other Kraus–Turner models (KTB and KTC) are used, all shortwave radiation is absorbed within the mixed layer. Penetrating shortwave radiation is always used in the three differential models (KPP, GISS and MY) along with the PWP model.

Surface heat and mass fluxes are distributed over model layers within the individual vertical mixing algorithms. The vertical momentum fluxes at the surface (wind stress) and at the bottom (bottom stress) are always applied prior to solving the HYCOM baroclinic momentum equation. The surface momentum flux is distributed over model layer 1, thus accelerating fluid in that layer only. The bottom flux is distributed over the bottom 10 m of the water column, and thus accelerates fluid only in those layers that contain fluid within this depth range. The selected vertical mixing algorithm subsequently performs the momentum mixing.

2.4. Vertical mixing algorithms for hybrid coordinates

2.4.1. *K-Profile Parameterization*

The KPP (Large et al., 1994, 1997) model provides mixing from surface to bottom, smoothly matching the large surface boundary layer diffusivity and viscosity profiles to the relatively weak diapycnal diffusivity and viscosity profiles of the interior ocean. It works on a relatively coarse and unevenly spaced vertical grid, and it parameterizes the influence of a larger suite of physical processes than other commonly used mixing schemes. In the ocean interior, the contribution of background internal wave breaking, shear instability mixing, and double diffusion (both salt fingering and diffusive instability) are parameterized. In the surface boundary layer, the influences of wind-driven mixing, surface buoyancy fluxes, and convective instability are parameterized. The KPP algorithm also parameterizes the nonlocal mixing of T and S , which permits the development of countergradient fluxes.

The KPP model is semi-implicit, requiring multiple iterations. The procedure for mixing thermodynamical variables and scalar tracers at p grid points is summarized as follows: first, the velocity components carried at u and v grid points are horizontally interpolated to p points. For the first iteration, vertical profiles of T and S diffusivity coefficients along with viscosity coefficients are calculated at model interfaces from the initial profiles of model variables. A tri-diagonal matrix system is formulated to solve the one-dimensional vertical diffusion equation following the procedures developed by Large et al. (1994). For the second iteration, the vertically mixed profiles of model variables on the p points are used to estimate new profiles of viscosity and T , S diffusivity profiles, which are then used to mix the original profiles of model variables. This procedure is repeated until the mixed profiles of model variables differ insignificantly from the mixed profiles obtained from the previous iteration. Tests revealed that two iterations are generally sufficient. After calculating the final viscosity and diffusivity profiles, T , S , and other model scalars stored at p grid points are vertically mixed. To mix momentum components, viscosity profiles stored at p points are horizontally interpolated to u and v grid points, then the vertical diffusion equation is solved on both sets of grid points. Further details of the implementation of KPP mixing in HYCOM are presented in the HYCOM Users Manual (Bleck et al., 2002).

2.4.2. *NASA/GISS level 2 turbulence closure*

The Goddard Institute for Space Studies (GISS; Canuto et al., 2001, 2002) model is a level 2 Reynolds stress model where viscosity and T , S diffusivities are parameterized as functions of Brunt–Vaisala frequency, the gradient Richardson number Ri^T , the turbulent kinetic energy dissipation rate, and a density ratio $R_\rho = \alpha \partial T / \partial z (\beta \partial S / \partial z)^{-1}$. The GISS model parameterization is valid for the following four cases (Canuto et al., 2002): doubly stable ($\partial T / \partial z > 0$, $\partial S / \partial z < 0$, $R_\rho < 0$, $Ri^T > 0$), doubly unstable ($\partial T / \partial z < 0$, $\partial S / \partial z > 0$, $R_\rho > 0$, $Ri^T < 0$), salt fingering ($\partial T / \partial z > 0$, $\partial S / \partial z > 0$, $R_\rho > 0$, $Ri^T > 0$), and diffusive convection ($\partial T / \partial z < 0$, $\partial S / \partial z < 0$, $R_\rho > 0$, $Ri^T > 0$). Equations for the second-order moments are solved to obtain viscosity and diffusivity coefficients (Canuto et al., 2002). Both large-scale (resolved) and small-scale (unresolved) shear contributes to the gradient Richardson number Ri^T . The model is solved differently in two regimes depending on whether resolved or unresolved shear has the dominant influence on stability. The former regime represents the intense mixing of the surface boundary layer while the latter represents the comparatively quiescent ocean interior. The boundary between the two regimes is

determined by whether Ri^T estimated from resolved shear alone exceeds a critical value. Different parameterizations of turbulent kinetic energy dissipation rate are used in these two regimes. Nonlocal effects are not parameterized.

After calculating the viscosity, T diffusivity, and S diffusivity profiles at p grid points, the same implicit procedure used to solve the vertical diffusion equation for the KPP model is invoked for the GISS model. After mixing at p grid points, viscosity profiles are horizontally interpolated to u and v grid points, then the vertical diffusion equation is solved for the momentum components on their native grids. Further details of the GISS model implementation are provided in the HYCOM Users Manual (Bleck et al., 2002).

2.4.3. Mellor–Yamada level 2.5 turbulence closure

The MY model (Mellor and Yamada, 1982; Mellor, 1998) is a level 2.5 Reynolds stress model adapted from the one-dimensional model embedded in the Princeton Ocean Model (POM) that solves the equations for q^2 (turbulence kinetic energy, or TKE) and q^2l (TKE times the turbulence length scale) to estimate the viscosity and diffusivity coefficient profiles. Since q^2 and q^2l are prognostic fields, POM contains code that horizontally advects and diffuses these fields, and also contains code that temporally averages the fields as part of the leapfrog time integration scheme. Only the one-dimensional model from POM has been implemented in HYCOM. Reliance is then placed on existing HYCOM algorithms to handle the other processes. Fluxes of q^2 and q^2l across model interfaces relocated by the hybrid grid generator are also calculated. The MY model is the only vertical mixing algorithm in HYCOM that accounts for the horizontal advection and diffusion of turbulence.

The greatest difficulty in implementing MY mixing in HYCOM arises from the different vertical grids that are used. In POM, fields of q^2 and q^2l are carried on model interfaces while HYCOM advection and diffusion algorithms operate on layer variables. The solution to this dilemma is to generate a new vertical grid to solve the one-dimensional MY equations and then carry q^2 and q^2l on both grids (Fig. 2). These two fields are carried as layer variables in all HYCOM routines except the MY model, to which they are passed directly as interface variables since MY grid interfaces are located at the central depths of HYCOM layers. This requires that other HYCOM layer variables be remapped as layer variables onto the MY vertical grid before solving the one-dimensional equations, and also that viscosity and diffusivity coefficients calculated on MY grid

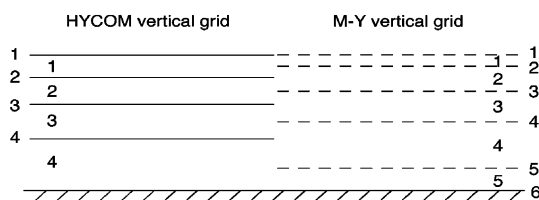


Fig. 2. The HYCOM vertical grid (left) and the special vertical grid used to store variables q^2 and q^2l for the MY mixing algorithm (right). Interface and layer numbers are shown for both grids. Variables q^2 and q^2l are stored as interface variables on the MY grid when the one-dimensional mixing algorithm is executed. Since the MY interfaces are located at mid-layer depths of the HYCOM vertical grid, q^2 and q^2l are passed as HYCOM layer variables to all other model algorithms, such as horizontal advection and diffusion and the vertical coordinate adjustment algorithm.

interfaces be remapped to HYCOM grid interfaces before solving the vertical diffusion equation using the same implicit procedure as the KPP and GISS models. As for the PWP and GISS models, viscosity profiles calculated at p grid points are horizontally interpolated to u and v points so that the vertical momentum diffusion equation is solved on the native grids. Details of the implementation of MY mixing are provided in the HYCOM Users Manual (Bleck et al., 2002).

2.4.4. Price–Weller–Pinkel dynamical instability model

In the Price et al. (1986) dynamical instability model adapted for HYCOM, vertical mixing at each grid point is performed in three steps: (1) static instability is relieved in the upper-ocean mixed layer if it exists, (2) mixed layer entrainment is performed based on a bulk Richardson number criterion, and (3) shear instability mixing between adjacent model layers is performed based a gradient Richardson number criterion. The complete model is executed at p grid points using momentum components horizontally interpolated from their native grids. To relieve static instability if present, water in layers 1 and 2 is completely mixed if layer 1 is denser than layer 2. After mixing, if the water in layer 3 is less dense than this mixed water, it is completely mixed with the water from layers 1 and 2. This process is repeated until a model layer is encountered that is denser than the mixed water above. An initial diagnosis of mixed layer thickness is performed next, being the depth of the first interface below the surface across which the density jump exceeds a prescribed value. The MLB always resides on a model interface in the PWP model. All model variables are then homogenized within the mixed layer.

The bulk Richardson number is then calculated using density and velocity differences between the mixed layer and the model layer immediately below. If $R_b < 0.65$, the mixed layer entrains that layer and all variables are homogenized within the new mixed layer. The process is then repeated, with the mixed layer entraining additional layers, until $R_b \geq 0.65$.

The gradient Richardson number is estimated at model interfaces, and mixing is performed using the following procedure: The number R_g is estimated at all vertical interfaces between the one upon which the MLB resides and bottom of the deepest layer with nonzero thickness. The interface with the smallest value of R_g is identified. If this value is less than 0.25, the layers above and below the interface are partially mixed so that the value of R_g is increased to 0.30. New values of R_g are calculated, and then the new interface with the smallest value of R_g is identified. If this value is less than 0.25, the two adjacent layers are partially mixed in the same manner. This process is repeated until the minimum value of R_g over all layers exceeds 0.25.

After this mixing process has been completed, the depth of the MLB is again diagnosed as the depth of the first interface below the surface where the density jump exceeds a prescribed value. The final vertical homogenization is then performed for thermodynamical variables and other scalars stored at p grid points. The depth of the MLB is then horizontally interpolated to u and v grid points. On both sets of grids, the model interface closest to the interpolated mixed layer depth is identified as the MLB, and vertical homogenization of u and v is performed between the surface and the identified interface.

Although the PWP algorithm provides for shear instability mixing beneath the surface mixed layer, it does not provide for background mixing due to other processes such as internal wave breaking. When the PWP model is selected, the supplemental hybrid explicit (MICOM-like) diapycnal-mixing algorithm (Section 2.4.6), which does not contain a parameterization for shear instability mixing, is also activated to provide this additional mixing. Further details of the

HYCOM implementation of PWP are provided in the HYCOM Users Manual (Bleck et al., 2002).

2.4.5. Kraus–Turner mixed layer models for hybrid coordinates

The KT mixed layer is a vertically homogenized slab of water whose depth is diagnosed from the steady-state turbulence kinetic energy (TKE) equation, which assumes a balance between sources and sinks of TKE in the mixed layer. The TKE balance used in HYCOM is the same as the one used in MICOM (Bleck et al., 1989, 1992) and is therefore not discussed here. The greatest difficulty in incorporating a Kraus–Turner mixed layer model within a hybrid coordinate ocean model is to properly handle the MLB, the depth of which is a prognostic variable. Since the MICOM slab mixed layer is identically layer one, the MLB always coincides with a model vertical coordinate. This is not true for hybrid coordinates, so special bookkeeping is required for MLB depth along with the discontinuities in properties that exist there. The buoyancy change across the MLB must be known to estimate terms of the TKE balance while jumps in other properties must be known to calculate their entrainment fluxes.

This situation is illustrated for temperature in Fig. 3. With the MLB found in model layer k between interface k above and $k + 1$ below, values of model layer variables between the MLB and interface k (upper sublayer) must equal the homogenized mixed layer values. Since the model carries vertically averaged values within layer k , a special “unmixing” algorithm is required to estimate values of model variables between the MLB and layer $k + 1$ (lower sublayer). During the

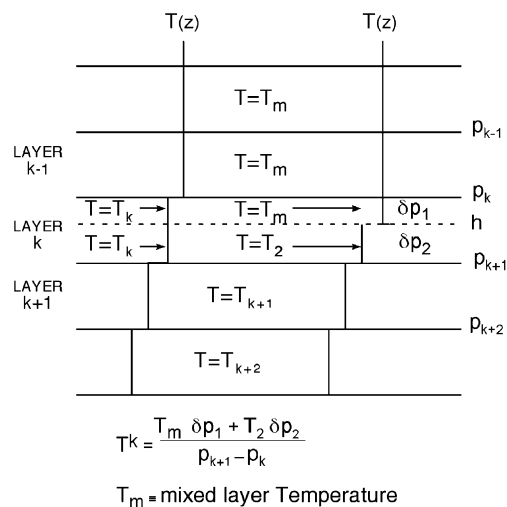


Fig. 3. Vertical distribution of a model layer variable (represented by T) in the hybrid KTA slab mixed layer model. The mixed layer base is located at pressure depth h within model layer k . The vertical distribution of T in the HYCOM vertical coordinate system is shown on left. In the vertical coordinate system used by the KTA model (right) model layer k has been divided into two sublayers above and below the mixed layer base with thicknesses δp_1 and δp_2 to enable the jumps in model variables across the base to be estimated. The value of T in the upper sublayer equals the homogenized mixed layer value. The unmixing algorithm described in the HYCOM Users Manual (Bleck et al., 2002) is used to determine the value of T in the lower sublayer (T_2) such that the thickness-weighted vertical average of the sublayer values equals the value of T_k .

development and testing of the unmixing scheme, it became clear that it had to be designed to reduce as much as possible numerically induced biases in property exchanges between the mixed layer and the deeper ocean. In test simulations of the Atlantic Ocean, it was found that model performance was very sensitive to unmixing errors in regions with weak stratification. Substantial effort was invested to make the unmixing algorithm as accurate as possible, which involves carrying sublayer variables at both leapfrog time steps so that previous values provide initial information for executing the unmixing algorithm at a new time step. This effort improved the realism of model simulations in the high latitude North Atlantic.

The primary KT model contained in HYCOM (KTA) uses this full unmixing algorithm to provide the most accurate possible update of mixed layer properties. This model has been equipped with a penetrating shortwave radiation option that permits part of this incoming radiation to penetrate beyond the MLB. Mixed layer convection is included, with the MLB moved downward to the next model interface if the mixed layer is denser than the lower sublayer. After this step, the mixed layer continues to entrain whole layers as long as the mixed layer is denser than the layer below. The complete KTA model is executed at p grid points by first homogenizing thermodynamical variables from the surface down to the new mixed layer depth. After homogenization, which alters the upper sublayer values, variables within the layer containing the MLB are re-calculated as a thickness-weighted average of the new upper and old lower sublayer values. The TKE balance is solved at this time. After relocating the MLB to its new depth, the new T , S profiles are calculated as follows. If entrainment has occurred, the variables are homogenized down to the new mixed layer depth and the vertically averaged values within the layer containing the MLB are re-calculated. If detrainment has occurred, values of T and S do not have to be re-calculated in any model layer, but the lower sublayer values must be recalculated.

The new mixed layer depths are interpolated to u and v grid points for momentum mixing. On each grid, the unmixing algorithm is then executed within the layer containing the MLB. Each momentum component is homogenized from the surface through the upper sublayer, and then new values are calculated for the layer containing the MLB as a thickness-weighted average of the new upper and old lower sublayer values. Technical details of KTA implementation are provided in the HYCOM Users Manual (Bleck et al., 2002).

To avoid the physical unreality of unmixing, and also for computational efficiency, Bleck (2002) developed a highly simplified KT model that avoids unmixing by making mixed layer thickness a diagnostic rather than a prognostic variable. This model (KTB) is also included in the current version of HYCOM and details of the implementation are provided in the HYCOM Users Manual (Bleck et al., 2002).

When either the KTA or KTB models are used, HYCOM relieves convective instability beneath the mixed layer by instantaneously homogenizing two layers when water in one layer is denser than water in the layer below. Since both the KTA and KTB models govern the surface mixed layer only, one of the two supplemental interior diapycnal mixing algorithms for hybrid coordinates provided in HYCOM must also be used.

2.4.6. Supplemental interior diapycnal mixing algorithms for hybrid coordinates

HYCOM is equipped with two supplemental interior diapycnal mixing algorithms to use with the slab mixed layer models for hybrid coordinates (Table 1). The first (explicit) model is a modified version of the MICOM version 2.8 algorithm. It works almost exactly as the MICOM

version, but the code has been modified to handle vertical resolution within the mixed layer. The second (implicit) model is essentially KPP with the surface boundary layer parameterization removed. The implicit model is preferred because in addition to background internal wave mixing, it also parameterizes mixing due to shear instability and double diffusion. Explicit interior diapycnal mixing is used to supplement the PWP model since shear instability mixing is already parameterized in that model. Following the MICOM convention, the explicit model does not mix momentum components. The implicit algorithm mixes momentum by first horizontally interpolating viscosity profiles to u and v grid points, then implicitly solving the vertical diffusion equation.

2.5. MICOM mode

When HYCOM is run in MICOM mode, the hybrid grid generator is not executed. Vertical mixing is performed using a third Kraus–Turner mixed layer model (KTC) that was imported from MICOM version 2.8 (Table 1). HYCOM is also equipped with a third supplemental interior diapycnal-mixing algorithm for use with isopycnic coordinates, specifically the MICOM 2.8 explicit algorithm (Table 1). As for MICOM, T and S are horizontally advected and diffused in layer 1 (the slab mixed layer), while S alone is horizontally advected and diffused in deeper layers with T diagnosed from the equation of state.

3. Experiments

The annual cycle of Atlantic Ocean circulation is simulated in a domain from 20S to 62N consisting of a square mesh on a Mercator projection with 2-degree zonal resolution and $2 \cos \phi$ degree meridional resolution, where ϕ is latitude (the same projection used in MICOM). The bottom topography is derived from a digital terrain dataset with 5' resolution in longitude and latitude (ETOPO5). The eight primary experiments are denoted by the abbreviations listed in Table 2. Seven model experiments are conducted with hybrid vertical coordinates that involve different vertical mixing choices, and these are compared to an eighth (MICOM mode) experiment. Six of the hybrid coordinate experiments are designed to highlight differences among the three differential mixing models (KPP, GISS, and MY) and the three slab mixed layer models for hybrid coordinates (PWP, KTAIP, and KTBI). The seventh hybrid experiment (KTAE) also uses mixed layer model KTA, but differs from experiment KTAIP by using explicit interior diapycnal mixing instead of implicit, and by not using penetrating shortwave radiation. Comparing experiments KTAIP and KTAE then illustrates the influence of penetrating shortwave radiation and shear instability mixing, neither of which is present in KTAE. Some additional experiments that are variants of these eight are also performed to address specific questions; they are described later as needed.

In all experiments, model potential density in sigma units is referenced to pressure at 20 MPa (~ 2000 m), and is referred to as σ_2 . The isopycnic reference densities used for all experiments are derived from Brydon et al. (1999) and listed in Table 3. The contribution of thermobaric compressibility (the influence of potential temperature anomaly on compressibility) is included in the calculation of horizontal pressure gradient by introducing the virtual potential density of Sun

Table 2

The eight primary model experiments, with names consisting of the mixed layer model abbreviation followed by “E” or “I” if an explicit or implicit supplemental interior diapycnal mixing model is also used

Experiment	Vertical coordinate	Mixed layer model	Supplemental diapycnal diffusion model	Penetrating shortwave radiation	Varb. Horiz. advected and diffused	Variables fluxed in grid generator
KPP	Hybrid	KPP	N/A	Yes	T, S	T, S
GISS	Hybrid	GISS	N/A	Yes	T, S	T, S
MY	Hybrid	MY	N/A	Yes	T, S	T, S
PWP	Hybrid	PWP	Explicit A	Yes	T, S	T, S
KTAIP	Hybrid	KTA	Implicit	Yes	T, S	T, S
KTBI	Hybrid	KTB	Implicit	No	T, S	T, S
KTAE	Hybrid	KTA	Explicit A	No	T, S	T, S
MIC	Isopycnic	KTC	Explicit B	No	σ_2, S	N/A

The letter “P” in experiment KTAIP signifies that penetrating shortwave radiation is switched on. MIC signifies MICOM mode, which uses model KTC. N/A means not applicable.

Table 3

Reference σ_2 for the eight primary experiments

Layer k	1	2	3	4	5	6	7	8	9	10	11
Refer σ_2	27.70	28.20	28.70	29.20	29.70	30.20	31.85	33.22	34.26	35.04	35.62
Layer k	12	13	14	15	16	17	18	19	20	21	22
Refer σ_2	36.05	36.37	36.61	36.79	36.92	37.01	37.07	37.11	37.14	37.17	37.20

et al. (1999). Including the thermobaric correction greatly reduces pressure errors at depths far from the reference pressure surface and produces more realistic wind-driven gyre circulation and thermohaline overturning circulation in HYCOM (Chassignet et al., 2003). The contribution of thermobaric compressibility to water column stability is included by using the locally referenced potential density instead of σ_2 to determine stability, calculate Richardson numbers, and solve the KT TKE balance. The minimum layer thicknesses δ_k are chosen to be 10 m in all layers. At each grid point, this minimum thickness is reduced to $\delta_{\min} = 2$ m in all layers that reside beneath the surface p coordinate domain to enable sharper pycnoclines to form in the interior ocean (Section 2.2). A 50–50 partition of Laplacian and biharmonic horizontal diffusion is employed. The baroclinic time step is 1.2 h while the barotropic time step is 3 min. Variables T, S are horizontally advected and diffused, and are also remapped by the hybrid grid generator. The sensitivity of results to this choice as opposed to ρ, S is explored to assess the tradeoff between the numerical cabbeling produced by the T, S choice and the non-conservation of T produced by the ρ, S choice (Section 4.3.4).

Monthly climatological surface fields of vector wind stress, wind speed, air temperature, air specific humidity, net shortwave radiation, net longwave radiation, and precipitation obtained from the COADS climatology are used to drive the model. At the northern and southern boundaries, model fields are relaxed to the WOA 1994 climatology (Levitus et al., 1994; Levitus

and Boyer, 1994) within a band that is six grid points wide. The inverse relaxation time scale increases linearly with distance away from the boundaries. A long time scale was chosen (20–120 days) to avoid driving excessive meridional overturning and associated heat flux. Although precipitation forcing is used, surface salinity is also relaxed to the WOA 1994 climatology to reduce the influence of biases and errors in the precipitation field.

For each experiment, the model is spun up from three-dimensional WOA 1994 climatology for 20 years. It is then run for one year beginning on day 16 (mid-January), and fields are saved every six days. Fields for day 46 (mid-February) represent boreal winter while those for day 226 (mid-August) represent boreal summer. All fields are horizontally smoothed using a two-dimensional Laplacian smoother to emphasize large-scale patterns. Model performance is evaluated by using the vertical mixing models “as is”. No attempts are made here to tune the large number of parameters contained in the models.

4. Results

4.1. Surface mixed layer

The slab models KTA and KTC (experiment MIC) carry mixed layer thickness as a prognostic variable determined from the TKE balance. The slab models PWP and KTB diagnose mixed layer thickness using their own algorithms. All three differential models (KPP, GISS AND MY) diagnose mixed layer thickness using the method of Kara et al. (2000a), which is implemented as follows: The user specifies a minimum temperature jump for estimating mixed layer thickness, which is converted to an equivalent density jump using the equation of state. The mixed layer base is located at the depth where density differs from layer 1 density by the value of this jump, which is estimated by linear interpolation of density between adjacent layers.

Winter (mid-February) mixed layer thickness patterns for the eight primary experiments (Fig. 4) are qualitatively similar. All models produce deep convection over part of the subpolar gyre, relatively strong convection off the coast of Europe and in the subtropical mode water (STMW) formation regions, thin mixed layers in the interior subtropical gyre, and somewhat thicker mixed layers in the North Atlantic Trade Wind belt. Good quantitative similarity throughout the Atlantic basin exists among the three differential models (KPP, GISS, MY). The deepest convection (>800 m) occurs in the Labrador Sea while relatively deep convection (\cong 600 m) extends eastward into the central subpolar gyre. Thicknesses of about 500 m exist off the coast of Europe, 200–400 m in the STMW formation regions, 100 m in the interior subtropical gyre, and about 150 m in the North Atlantic Trade Wind belt. The area where MLB depth exceeds 800 m is smaller in the GISS model than in the other two.

The MLB in the Labrador Sea and off the coast of Europe is deeper in experiment PWP compared to the three differential models. This is also true of the STMW formation region in the central and eastern parts of the basin. All of the KT experiments (KTAIP, KTBI, KTAE and MIC) tend to have less convection in the Labrador Sea, but substantially thicker mixed layers off the European coast and in the STMW formation regions. The detailed structure of MLB depth differs substantially in these regions among the KT experiments. The substantial differences between experiments KTAIP and KTAE primarily highlight the influence of shear instability mixing

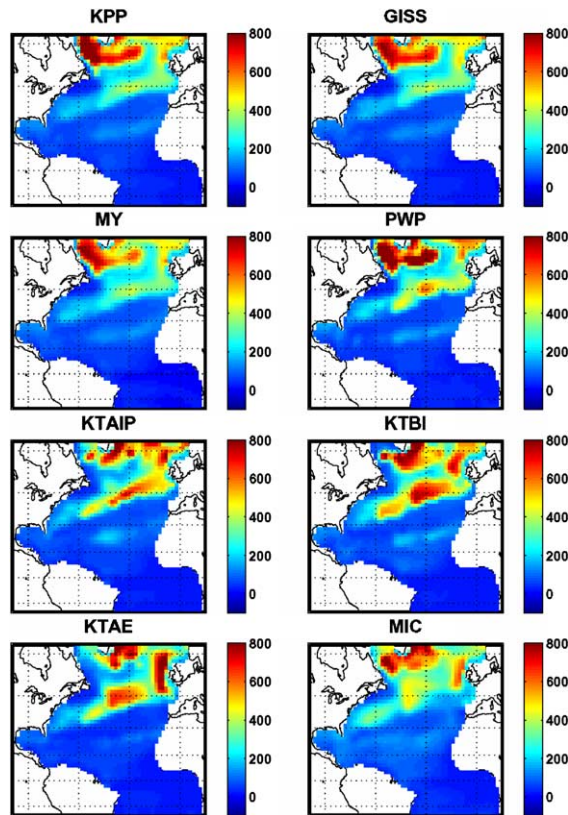


Fig. 4. Winter (mid-February) mixed layer thickness (m) for the eight primary experiments.

and penetrating shortwave radiation, neither being present in KTAE. Experiment KTAE is the only one of the eight that does not produce deep winter convection in the central Labrador Sea. Winter mixed layer thickness in convection regions is sensitive to the preconditioning of T , S profiles and to surface heat flux. Small changes in these properties resulting from the penetration of shortwave radiation can have a large influence on the annual cycle of mixed layer thickness.

Model variables at five grid points representing a wide range of oceanographic conditions (Fig. 5) are examined to further analyze vertical mixing, focusing on six of the eight primary experiments (KPP, GISS, MY, PWP, KTAIP, and MIC). The annual cycles of vertically averaged mixed layer temperature and mixed layer thickness are presented in Fig. 6 at these five points. Substantial disagreement among the experiments is evident at point EQTR. The three differential mixing models KPP, GISS, and MY plus KTAIP produce similar annual cycles of mixed layer T . Experiment MIC produces comparatively warm T during the last half of the year. The MIC equatorial cold tongue forms during spring as in the previously mentioned experiments, but decays rapidly during middle and late summer. Experiment PWP maintains a stronger cold tongue than the other five experiments throughout the year. The mixed layer thickness tends to be larger for PWP than for the other models. Since the PWP MLB always resides on a model interface, it

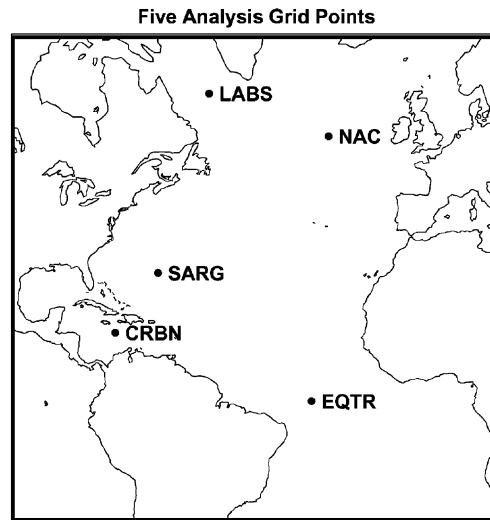


Fig. 5. Location of the five model grid points analyzed in detail. These points represent the equator (EQTR), the Trade Wind belt in the Caribbean Sea (CRBN), the interior subtropical gyre in the Sargasso Sea (SARG), the Westerly Wind belt in the North Atlantic Current (NAC), and the deep convection region of the Labrador Sea (LABS).

occasionally toggles between the two interfaces bounding the first thick layer located beneath the p coordinate domain.

In the Trade Wind belt and interior subtropical gyre (points CRBN and SARG), all experiments produce very similar annual cycles of SST (Fig. 6), with the most noticeable outliers being experiment KTAIP, which is slightly colder than the other experiments during summer at point CRBN, and experiment MIC, which is relatively warm at point SARG during summer. Experiment MIC produces a much thicker mixed layer at point CRBN throughout the year than the other experiments. The annual MLB cycle at point SARG is generally similar among the six experiments except that the PWP and KTAIP winter mixed layers are not as thick as the other experiments. In the Westerlies (point NAC), annual cycles of SST are similar except for the relatively warm winter values produced by PWP and KTAIP. This difference occurs because the NAC path is displaced farther northward in these two experiments. Annual cycles of thickness are similar except that the winter maximum is relatively small for KPP and large for MIC. In a deep convection region (point LABS), the annual cycles of SST are similar except for MIC, which produces relatively warm values during the last half of the year. Winter thicknesses differ by up to about 50%, with PWP being the deepest and KTAIP being the shallowest over most of the winter. At all five points, experiment MIC is observed to be an outlier more often than the other experiments.

Winter upper-ocean profiles of viscosity K_M and T diffusivity K_T for the three differential models (Fig. 7) illustrate local differences among the models. At point EQTR, where forcing is stable (strong surface heating) and wind stirring plus shear instability largely produce vertical mixing, the GISS model produces substantially smaller K_M , K_T values than the others. Both KPP and MY produce large K values above 50 m. The KPP model also produces large values at one model interface located between 60 and 70 m, resulting from shear instability mixing between the

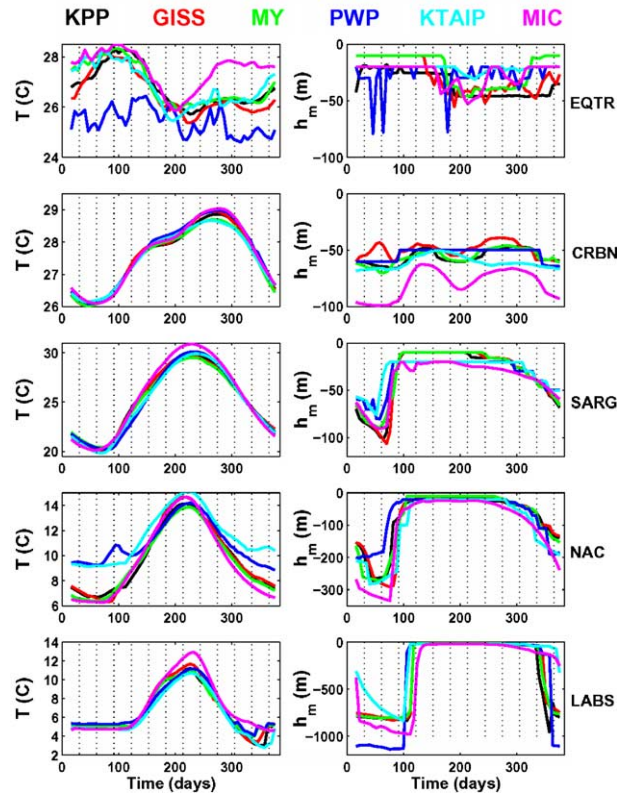


Fig. 6. Time series of vertically averaged temperature in the mixed layer (left) and the thickness of the mixed layer (right) at the five analysis grid points. Time series are presented for six of the primary experiments, and they are distinguished by the colors of the experiment names at the top.

westward South Equatorial Current above and the eastward Equatorial Undercurrent below. At point CRBN, all three experiments produce large K values in the mixed layer, with MY being largest and KPP smallest. The GISS model produces a thinner mixed layer, so large K values are confined closer to the surface. At point SARG, model KPP produces smaller K values in the mixed layer than the other two models. At the two northernmost points NAC and LABS, model GISS tends to produce larger K values in the mixed layer than the other two models. The large values produced by MY mixing extend deeper into the water column than for the other two models. At the three grid points with the thickest mixed layers (SARG, NAC and LABS), models KPP and MY produce smooth K profiles while the profiles produced by GISS exhibit substantial small-scale vertical structure. The K values representing background mixing at the top of the relatively quiescent ocean interior are also evident in Fig. 7. With no shear instability mixing and no double diffusion, these values are fixed at $K_M = 10^{-4}$ and $K_T = 10^{-5}$ m²/s for KPP. The GISS and MY models produce smaller K_M values than KPP. The GISS model produces very similar K_T values to KPP while the MY model produces somewhat larger values.

The use of differential vertical mixing models permits HYCOM to resolve both geostrophic shear and the shear of the ageostrophic wind-driven flow within the mixed layer. Since the model

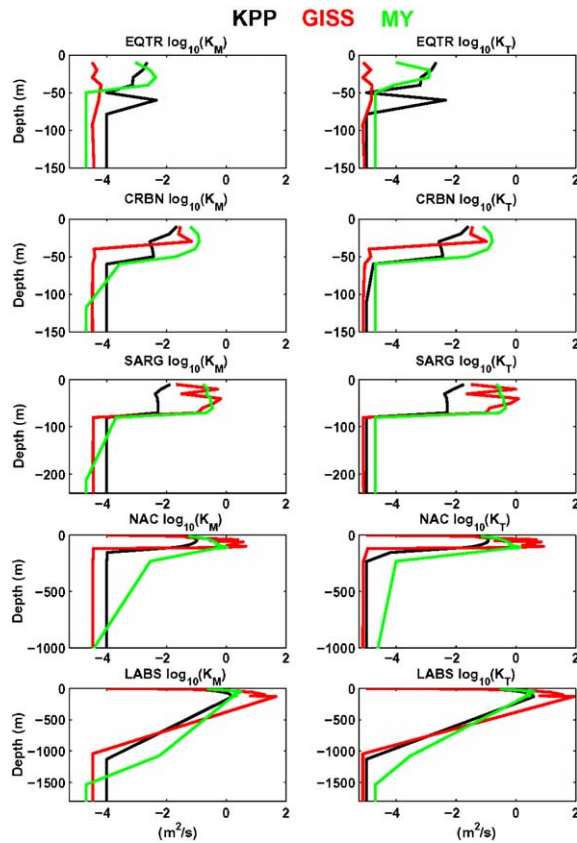


Fig. 7. The winter (mid-February) base-10 logarithm of viscosity (left) and temperature diffusivity (right) at the five analysis grid points for the three experiments that use differential mixing models. The experiments are distinguished by the colors of the names at the top.

is driven by slowly varying monthly climatological wind stress, a well-defined surface Ekman spiral should exist in experiments KPP, GISS, and MY. This expectation is verified at grid points CRBN and NAC in the Trade Wind and Westerly Wind belts, respectively (Fig. 8). To resolve the structure of the spiral with reasonable detail, and to make sure that the Ekman layer is confined to the p coordinate domain, special experiments were run with 10 additional light layers added at the top of the water column to the 22 layers used for the primary experiments. The specified minimum thickness is 3 m in the surface layer, and it increases slowly with depth to reach 15 m by layer 17. To generate the plots in Fig. 8, the model layer representing the base of the Ekman layer is identified by visual inspection of velocity vector plots, and then the velocity within this reference layer is subtracted from the velocity in the layers above. The resulting winter velocity vectors above the base of the Ekman layer (Fig. 8) demonstrate that the three differential models produce very similar Ekman spirals. Although geostrophic velocity shear is present in all of the velocity profiles in Fig. 8, it is too small to mask the Ekman spiral structure.

The central depths of the reference layers (the base of the Ekman layer) can be used as a proxy for Ekman layer thickness so that it can be compared among the cases that are plotted. (The

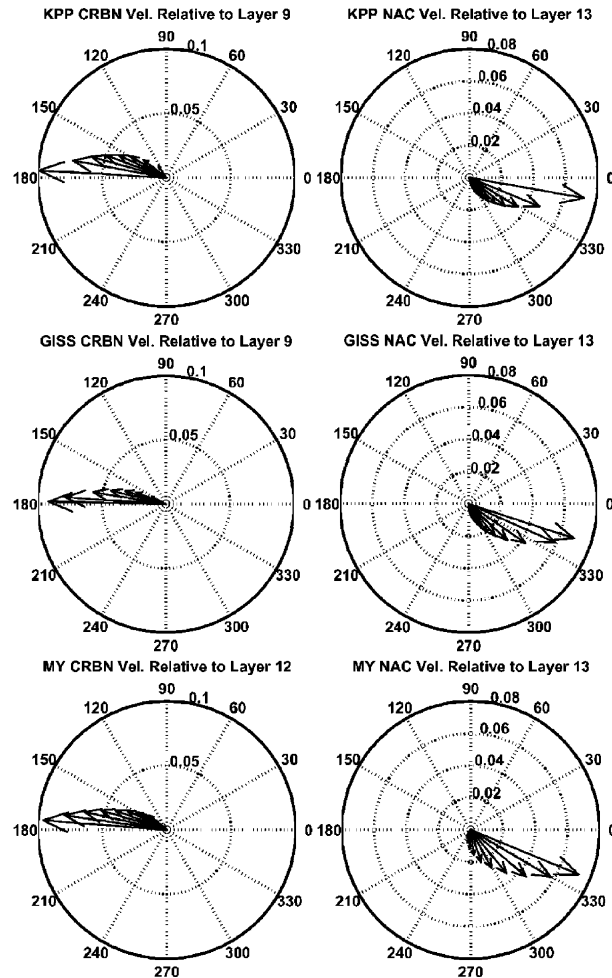


Fig. 8. Winter (mid-February) velocity vectors (m/s) at two grid points: CRBN (left) and NAC (right) obtained from three special experiments where 10 additional light layers have been added to the KPP (top), GISS (middle) and MY (bottom) experiments. Vectors are shown for model layers located above a reference layer shown in the label of each panel and chosen by inspection to reside at the Ekman layer base. The reference layer velocity has been subtracted from all vectors in each panel.

theoretical Ekman layer thickness is an e-folding scale.) At point CRBN, the MY Ekman layer is thicker than the KPP and GISS Ekman layers (67 m versus 41 m central depths) because the MY model produces larger viscosity values. The NAC Ekman layers are equally thick (78 m central depth) for all mixing models and thicker than all of the CRBN Ekman layers. Although the larger Coriolis force acts to reduce Ekman layer thickness at higher latitudes, the larger viscosity present at point NAC more than compensates for this reduction.

The previous discussion demonstrates that the vertical mixing choices in HYCOM can produce substantial differences in local mixed layer behavior. The all-important question is how do these differences impact the simulation of important ocean processes acting over large scales. The

impact of the choices on the wind-driven circulation will be documented first, and then the impact on thermohaline processes will be evaluated.

4.2. Impact of vertical mixing and vertical coordinate choices on wind-driven circulation

In the open ocean away from strong boundary currents, the barotropic flow should be quasi-Sverdrupian; i.e., a function of the wind stress curl pattern and independent of the baroclinic structure of the ocean. The open-ocean barotropic flow simulated by HYCOM should therefore be nearly independent of the vertical mixing and vertical coordinate choices as long as they are properly implemented within the model. Barotropic streamfunction maps for two of the eight primary experiments (KPP, MIC; Fig. 9) reveal very similar structure with boundaries between gyres following realistic paths. Open ocean streamfunctions in the subtropical and subpolar gyres are roughly consistent with Sverdrup dynamics. Patterns for the other six hybrid coordinate experiments are very close to the KPP pattern (not shown). The sea surface height (SSH) maps for two of the eight primary experiments (KPP, MIC; Fig. 9) display surface quasi-geostrophic flow patterns that are quite realistic for low-resolution simulations. Patterns for the other six hybrid coordinate experiments are also very close to the KPP pattern (not shown). In particular, the path of the Gulf Stream and North Atlantic Current are very reasonable. The Gulf Stream separates from the coast at Cape Hatteras to allow the existence of a slope water gyre. As the Gulf Stream flow reaches 50°W, it turns northward, and then eastward near the Flemish Cap as it does in nature. The northward flow of warm water in the eastern subpolar gyre is reproduced reasonably well.

Neither the vertical coordinate or vertical mixing choices have a large influence on wind-driven barotropic and baroclinic flow patterns. It will be demonstrated that thermohaline processes are more sensitive to these choices in low-resolution climate simulations.

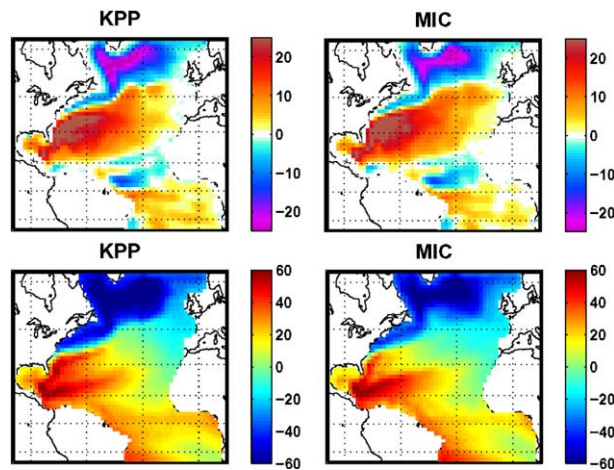


Fig. 9. Winter (mid-February) barotropic streamfunction (Sv) (top row) along with sea surface height ($m \times 100$) (bottom row) for two of the eight primary experiments (KPP and MIC). Mean SSH has been subtracted from both bottom panels.

4.3. Impact of vertical mixing and vertical coordinate choices on thermohaline processes

4.3.1. Winter and summer SST patterns

The winter (mid-February) SST field for the KPP reference experiment is presented in Fig. 10 along with SST difference fields between the seven other primary experiments and KPP, the latter illustrating model sensitivity to vertical mixing and coordinate choices. The rms amplitudes of these difference fields are listed in Table 4. The simulated winter SST field differs least for the three differential mixing models (KPP, GISS and MY) and PWP. Larger differences are observed for the KT experiments (KTAIP, KTBI, KTAE and MIC). The closest SST resemblance is observed

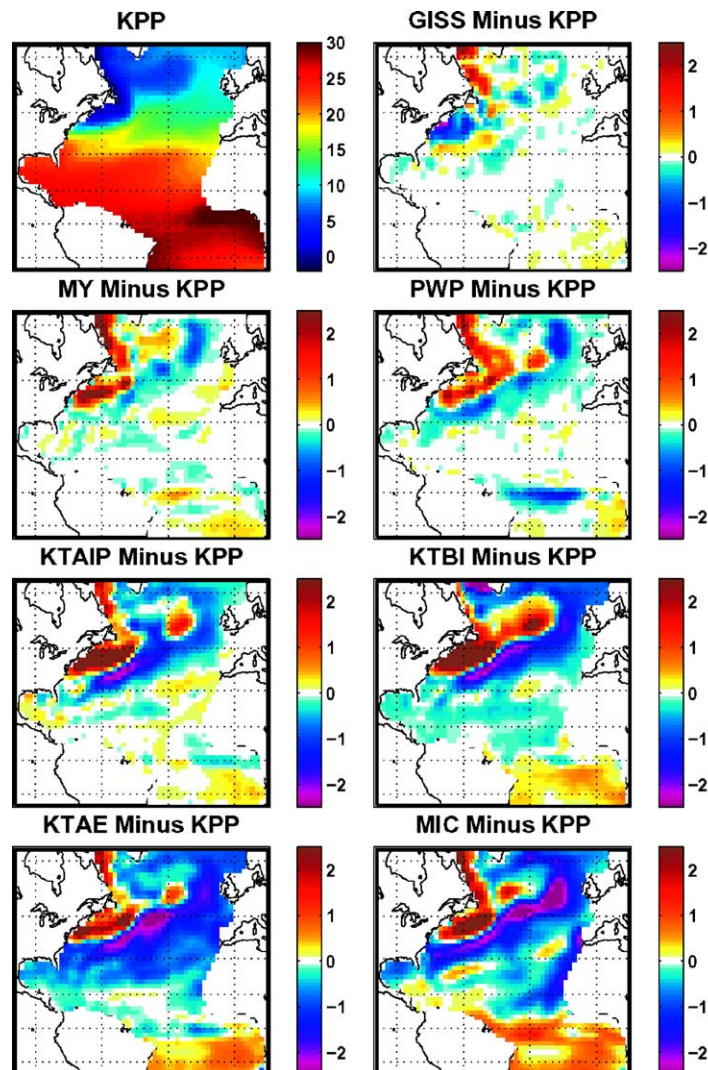


Fig. 10. Winter (mid-February) surface layer temperature ($^{\circ}\text{C}$) for experiment KPP along with difference maps between the other seven primary experiments and KPP. Warm colors indicate that the second experiment is warmer than KPP.

Table 4

RMS differences in several fields between seven of the eight primary experiments and experiment KPP, which was arbitrarily chosen as the reference experiment

Experiment	Winter Sfc. layer temp. (°C)	Summer Sfc. layer temp. (°C)	Winter Sfc. heat flux (W/m ²)	Summer Sfc. heat flux (W/m ²)	Winter σ_2 29W cross- section (0–500 m)	Winter σ_2 29W cross- section (0–4000 m)
GISS minus KPP	0.33	0.26	19.7	9.1	0.10	0.05
MY minus KPP	0.50	0.16	20.2	7.5	0.16	0.07
PWP minus KPP	0.49	0.22	19.8	10.5	0.14	0.07
KTAIP minus KPP	0.78	0.28	36.0	11.5	0.18	0.09
KTBI minus KPP	1.04	0.41	47.9	14.2	0.19	0.09
KTAE minus KPP	0.95	0.82	33.4	12.6	0.20	0.10
MIC minus KPP	1.02	0.76	39.2	13.9	0.34	0.15

between KPP and GISS, where the rms difference is 0.33 °C. The largest differences between these two experiments exist in the western Labrador Sea where GISS is warmer than KPP, and in the slope water gyre where GISS is colder. Open ocean differences between these two experiments are very small (Fig. 10). Slightly larger rms differences are observed between MY and KPP (0.50 °C) and between PWP and KPP (0.49 °C). In MY and PWP, both the western Labrador Sea and the slope water gyre are warmer than KPP while in PWP, the equator is colder than KPP (see Fig. 6). Rms differences between KT experiments and KPP are 0.78 °C for KTAIP, 1.04 °C for KTBI, 0.95 °C for KTAE, and 1.02 °C for MIC. All four of these experiments are much warmer than KPP in the western Labrador Sea and slope water gyre, and are colder than KPP to the south of the path of the Gulf Stream and North Atlantic Current. Experiment KTAIP displays the smallest open-ocean differences from KPP compared to the other three KT experiments. Experiments KTBI, KTAE, and MIC all tend to be colder than KPP in the open ocean north of the equator and warmer than KPP to the south. These three experiments do not use penetrating shortwave radiation. The overall difference patterns from KPP are quite similar for KTAE and MIC, the former being the hybrid experiment with vertical mixing most similar to MIC. These facts suggest that the SST differences between MIC and KPP are largely due to: (1) the different performance characteristics of the KT mixed layer model with respect to KPP, and (2) the absence of penetrating shortwave radiation and shear instability mixing in the KTC mixed layer model. The vertical coordinate choice (hybrid versus isopycnic) appears to have a relatively minor influence on winter SST. Rockford et al. (2001) demonstrated that including penetrating shortwave radiation (discussed further in Section 4.3.5) has a positive impact on the performance of the Kraus–Turner mixed layer model.

The SST differences contribute to differences in surface heat flux (Table 4). As for SST, the smallest rms differences in surface heat flux occur between KPP and both GISS and MY, typically about 20 W/m². Larger differences up to 47.9 W/m² are observed between KPP and the experiments using slab mixed layers. All of these observed heat flux differences are sufficiently large for the vertical mixing choice to matter in ocean climate simulations.

The summer (mid-August) SST field for KPP, along with SST difference fields between the seven other primary experiments and KPP, are presented in Fig. 11. The rms amplitudes of these

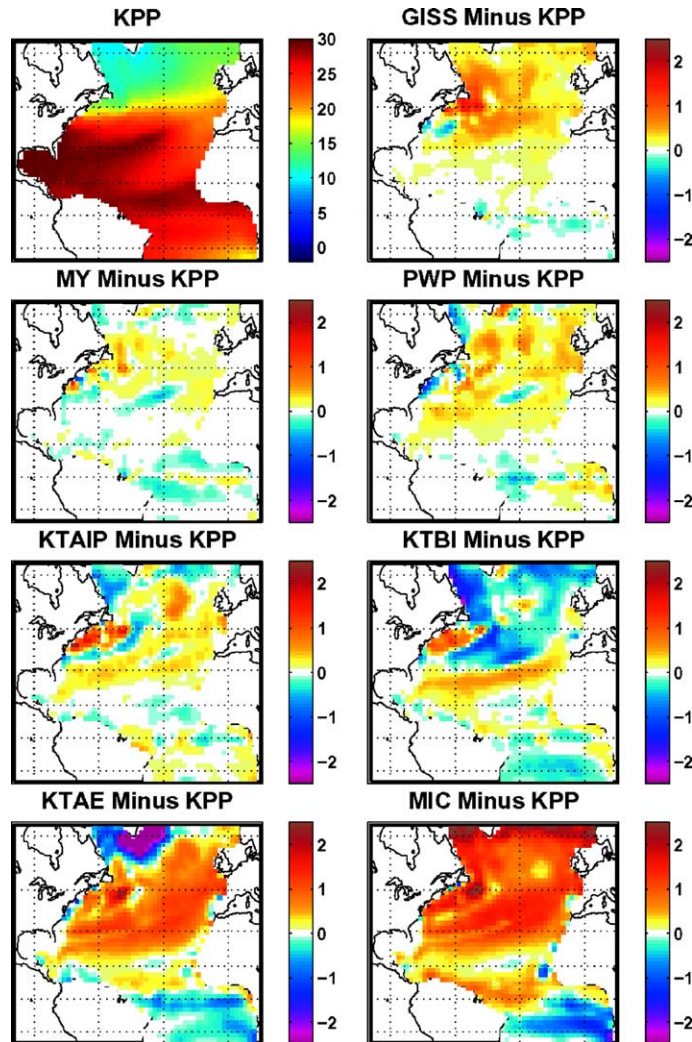


Fig. 11. Summer (mid-August) surface layer temperature ($^{\circ}\text{C}$) for experiment KPP along with difference maps between the seven other primary experiments and KPP. Warm colors indicate that the second experiment is warmer than KPP.

difference fields are listed in Table 4. Four experiments (GISS, MY, PWP and KTAIP) show substantially smaller differences from the KPP experiment than experiments KTAE and MIC, while experiment KTBI shows intermediate differences. Experiment MY most closely resembles KPP with an rms difference of $0.16\text{ }^{\circ}\text{C}$. Both GISS and PWP tend to be a little warmer than KPP north of about 20°N , and have rms differences from KPP of 0.26 and $0.22\text{ }^{\circ}\text{C}$, respectively. The large rms differences of both experiments KTAE and MIC from KPP (0.82 and $0.76\text{ }^{\circ}\text{C}$, respectively) have generally similar patterns except in the northwestern subpolar gyre, being warmer than KPP in the northern hemisphere and colder in the southern hemisphere. Since this pattern is present in experiment KTAE but not KTAIP suggests that penetrating shortwave radiation may be largely responsible for the warmer SSTs in the northern hemisphere due to the

absorption of all incoming shortwave radiation in the shallow summer mixed layer. Experiment KTBI produces deeper summer mixed layers than the other Kraus–Turner experiments (not shown), so it does not produce excessive northern hemisphere warming. As for winter SST, vertical coordinate choice probably makes a relatively minor contribution to the large differences between MIC and KPP.

The smallest summer rms differences in surface heat flux (Table 4) associated with SST differences occur between KPP and both GISS and MY, as was the case for winter, and are $<10 \text{ W/m}^2$. Differences exceeding 10 W/m^2 are observed between KPP and the other experiments that use slab mixed layers.

Maps of winter and summer SST differences between the eight simulations and the WOA 1994 climatology (the same climatology used for initial conditions) are presented in Figs. 12 and 13,

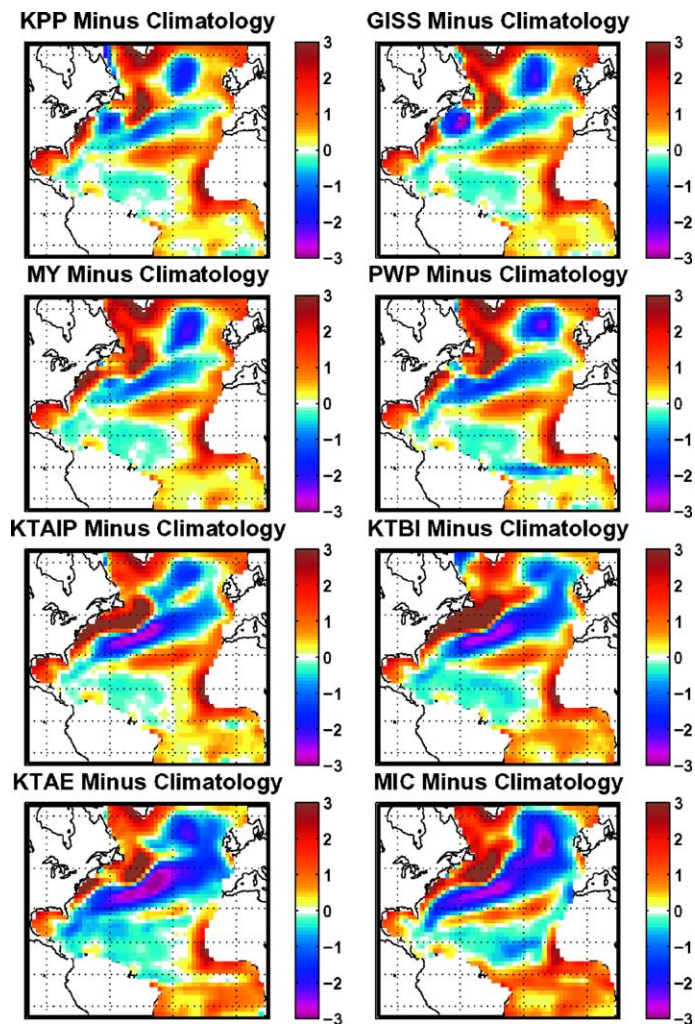


Fig. 12. Winter (mid-February) surface layer temperature difference ($^{\circ}\text{C}$) between the eight primary experiments and WOA94 climatology. Warm colors indicate that simulated temperature is warmer than climatology.

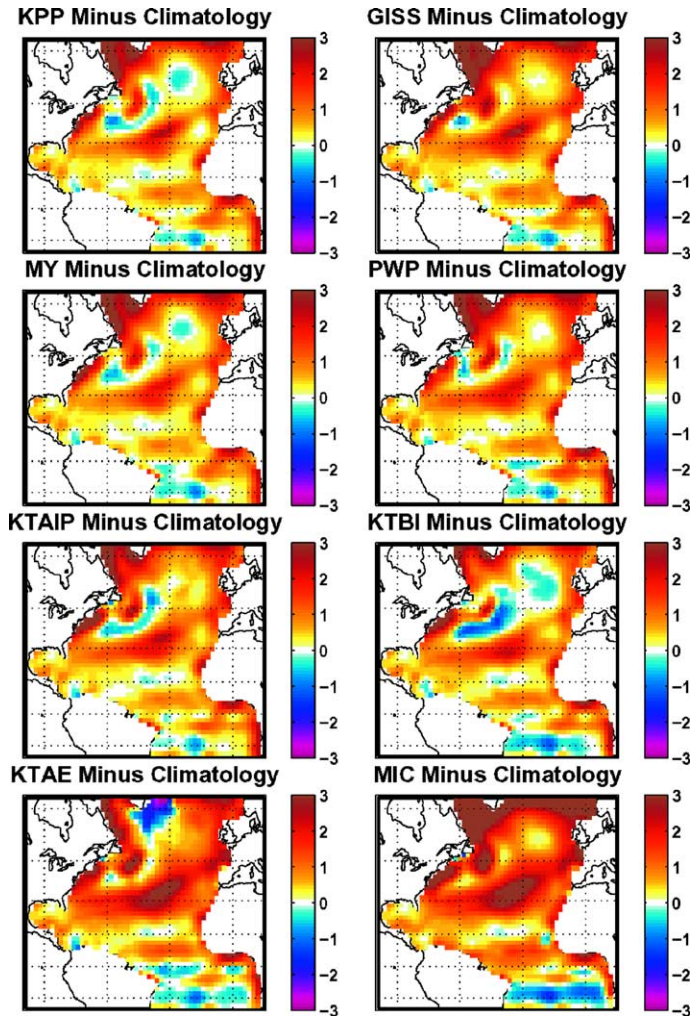


Fig. 13. Summer (mid-August) surface layer temperature difference ($^{\circ}\text{C}$) between the eight primary experiments and WOA94 climatology. Warm colors indicate that simulated temperature is warmer than climatology.

respectively, with rms differences tabulated in Table 5. Experiments KPP, GISS, MY, and PWP display very similar winter difference patterns from climatology (Fig. 12). The rms differences for these experiments range from $0.90\text{ }^{\circ}\text{C}$ (KPP) to $1.05\text{ }^{\circ}\text{C}$ (PWP) (Table 5), which is between two and three times larger than the rms differences observed between KPP and the other three experiments (Table 4). The observed differences between winter SST and climatology result primarily from factors other than vertical mixing choice for these four experiments (e.g. forcing errors, low model resolution, and parameterization of other model processes). The other four experiments (KTAIP, KTBI, KTAE and MIC) have larger rms differences from climatology, with values ranging between 1.20 and $1.36\text{ }^{\circ}\text{C}$ (Table 5). Comparing this to SST differences from KPP (Table 4), vertical mixing makes a much larger relative contribution to the observed SST differences from climatology in these four experiments.

Table 5
RMS differences between simulated and climatological fields for the primary experiments

Experiment	Winter surface temperature (°C)	Summer surface temperature (°C)	Winter 29W σ_2 cross-section (0–500 m)	Winter 29W σ_2 cross-section (0–4000 m)
KPP	0.90	0.82	0.26	0.12
GISS	0.96	0.88	0.27	0.12
MY	0.97	0.81	0.28	0.13
PWP	1.05	0.81	0.26	0.13
KTAIP	1.20	0.82	0.26	0.14
KTBI	1.36	0.80	0.27	0.13
KTAE	1.23	0.99	0.24	0.14
MIC	1.30	1.33	0.31	0.15

For all experiments, subpolar water in the western part of the basin is too warm while water in the northern subtropical and eastern subpolar gyres tends to be too cold. The amplitude of this pattern is largest in the four models that use KT mixed layers (KTAIP, KTBI, KTAE and MIC). The simple ice model may contribute to SST errors in the western subpolar gyre. Another region with large SST differences from climatology in all eight experiments is located offshore of the northwest Africa coastal upwelling region. SST may be too warm there because the low-resolution simulation does not adequately resolve physical processes associated with coastal upwelling.

From the summer SST difference patterns between simulations and climatology (Fig. 13), all vertical mixing choices produce SST that is too warm over nearly the entire northern (summer) hemisphere. This warm bias is largest for experiments KTAE and MIC, with rms differences of 0.99 and 1.33 °C, respectively, because all shortwave radiation is absorbed within the shallow summer mixed layer. In comparison, the rms differences for the other six experiments range from 0.80 to 0.88 °C (Table 5). Although experiment KTBI also does not have penetrating shortwave radiation, it produces a summer mixed layer that is too thick and thus distributes the trapped shortwave radiation over a larger depth range and limits overheating. All mixing models tend to overheat the summer mixed layer. It is possible that the use of high frequency forcing that resolves synoptic and diurnal variability will improve this situation.

4.3.2. Annual cycle of SST

In all experiments, correlation coefficients between the simulated and climatological annual cycles of SST exceed 0.95 over nearly the entire domain (not shown). As a result, the skill score Σ (Murphy, 1988) is used to evaluate the quality of SST annual cycle simulations:

$$\Sigma = r^2 - [r - (\sigma_Y/\sigma_X)]^2 - [(\bar{Y} - \bar{X})/\sigma_X]^2, \quad (1)$$

where r is the correlation coefficient and \bar{X} (\bar{Y}) and σ_X (σ_Y) are the means and standard deviations of the simulated (climatological) fields. From the rightmost two terms of (1), the skill score takes into account whether the simulated annual cycle has correct amplitude and mean value. If these are exactly correct, then Σ equals the square of the correlation coefficient. Differences between the means and rms amplitudes can decrease Σ to the point where it becomes negative. The skill is considered to be significant if $\Sigma > 0$.

Maps of the skill score are presented for the eight primary experiments in Fig. 14. For presentation purposes, negative Σ values are set to zero so that values ranging from zero to one are mapped. Domain averages of the skill score are tabulated in Table 6 and range from 0.73 to 0.77 for experiments KPP, GISS, MY, PWP, KTAIP, and KTBI. The scores for the other two experiments are smaller, being 0.63 for experiment KTAE and 0.47 for experiment MIC. The large-scale Σ patterns in Fig. 14 clearly show that high skill scores are present over a smaller fraction of the domain in experiments KTAE and MIC. In general, insignificant skill scores are present in the Labrador Sea and in a narrow band crossing the tropical Atlantic. These regions are largest in experiment MIC. The skill score becomes insignificant in a small region in the center of the subtropical gyre in experiments KTBI, KTAE, and MIC. The other experiments show a minimum in skill score in this region that does not become insignificant. This spot is a region

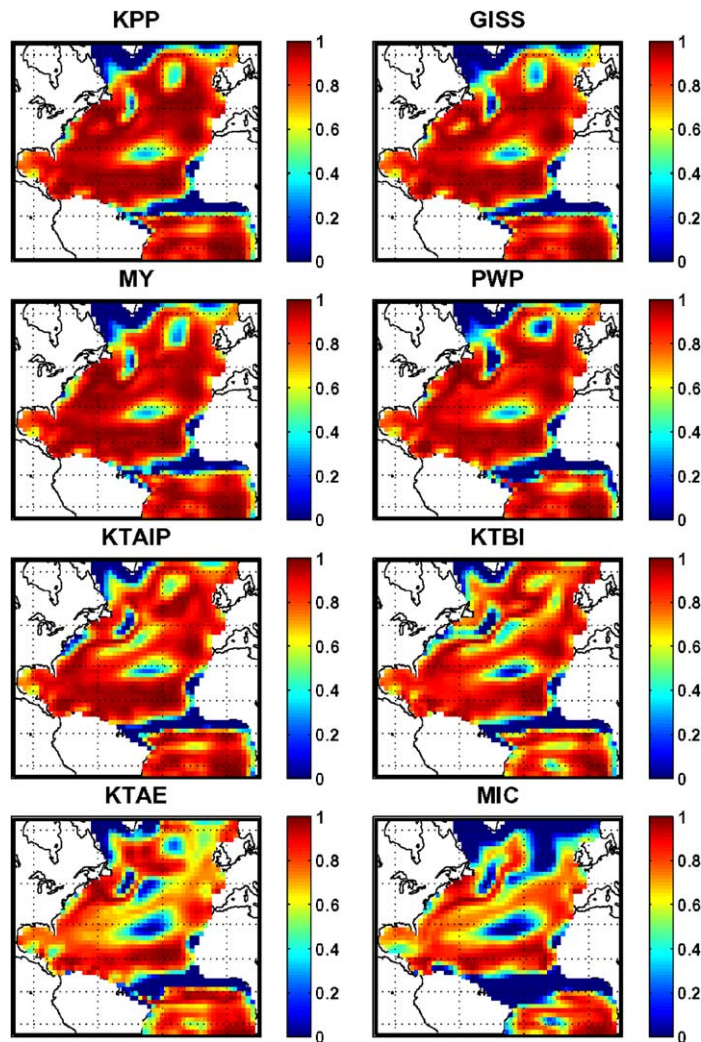


Fig. 14. Skill scores calculated from Eq. 1 for the simulated surface layer temperature (SST) annual cycle.

Table 6

Evaluation of the simulated SST annual cycle and climatology. The correlation coefficients and skill scores have been averaged over all model grid points

Experiment	Correlation coefficient	Skill score
KPP	0.99	0.77
GISS	0.98	0.74
MY	0.98	0.76
PWP	0.98	0.73
KTAIP	0.98	0.77
KTBI	0.98	0.73
KTAE	0.98	0.63
MIC	0.97	0.47

where the summer mixed layer tends to become very overheated (Fig. 13). Overall, this analysis demonstrates that the accuracy with which climatological SST is simulated is improved when we move from isopycnic to hybrid coordinates and include improved turbulence closure schemes.

4.3.3. Subsurface baroclinic structure

The sensitivity of subsurface baroclinic structure to vertical coordinate and mixing choices is examined in winter meridional cross sections of σ_2 along 29 °W. The KPP cross-section for the upper 500 m, along with difference sections between the other seven primary experiments and KPP, are presented in Fig. 15. Rms magnitudes of these differences are listed in Table 4. To present these cross-sections, layer values of simulated and climatological σ_2 at all model grid points in the section of the water column are vertically re-gridded to a resolution of 2 m such that all vertical points between two model interfaces bracketing a layer are assigned the σ_2 value for that layer. The resulting field is horizontally interpolated to a 1° latitude resolution. It is these interpolated fields that are plotted in Fig. 15 and used to calculate rms differences.

For the σ_2 cross-sections in Fig. 15, the smallest rms difference between KPP and the other seven experiments (0.10) is observed for experiment GISS while the largest RMS difference (0.34) is observed for experiment MIC (Table 4). Experiments MY and PWP also have relatively small rms differences from KPP (0.16 and 0.14, respectively) while the other three (KTAIP, KTBI and KTAE) have larger differences (0.18, 0.19, and 0.20, respectively). The large rms difference between MIC and KPP is largely due to two factors: (1) the warm layer above 200 m in the tropical Atlantic is thinner in MIC compared to KPP, and (2) subtropical mode water between 30°N and 50°N is substantially denser (colder) in MIC (Fig. 15). Experiments KTAIP and KTAE are compared to help interpret these large differences. Experiment KTAE has neither penetrating shortwave radiation nor shear instability mixing, and thus most closely resembles the mixing in MIC. The warm layer in the tropical Atlantic is thinner and subtropical mode water is colder in KTAE than in KTAIP, suggesting that these two processes contribute to the MIC-KPP difference. To determine the contribution of each process, experiment KTAIP was repeated without penetrating shortwave radiation (not shown). Comparing this special experiment to KTAIP and KTAE demonstrates that the absence of shear instability mixing is primarily responsible for the thinner tropical Atlantic warm layer while the absence of penetrating shortwave radiation is primarily responsible for the cold mode water (see Section 4.3.5).

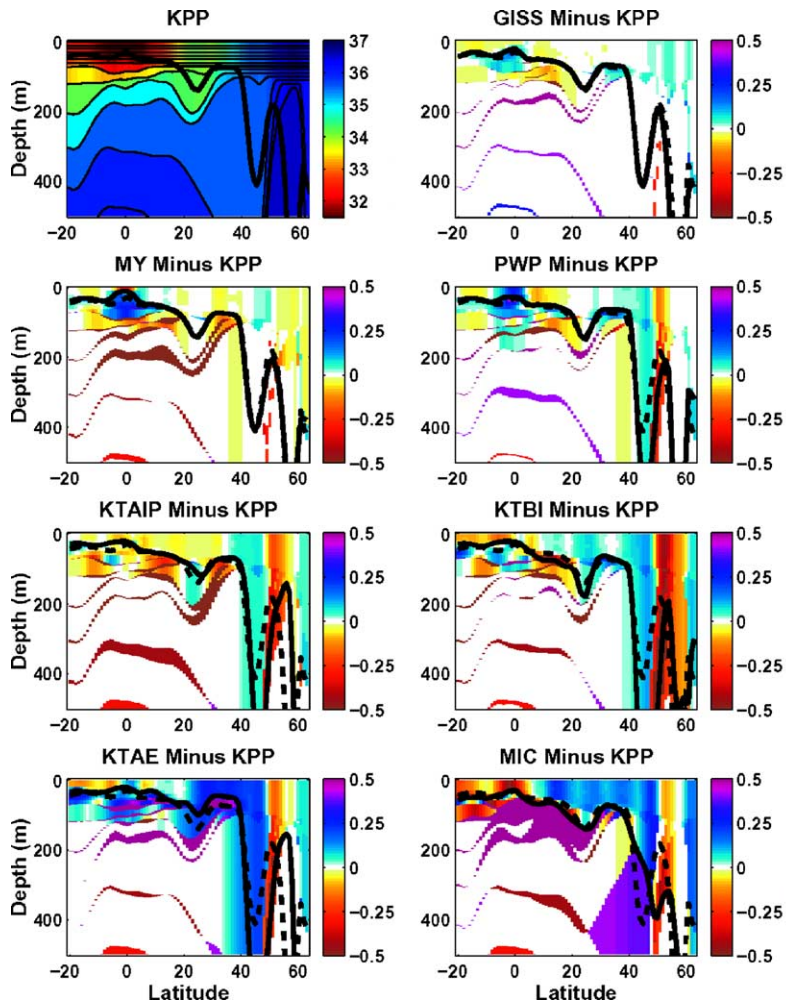


Fig. 15. Winter (mid-February) 29W cross-section of σ_2 in the upper 500 m of the water column for experiment KPP along with difference sections between the seven other primary experiments and KPP. Differences result from changes in interface depth in the isopycnic coordinate interior, but become “continuous” near the surface. The thick solid lines are the mixed layer base for each experiment while the thick dashed lines in the difference sections are the KPP mixed layer base. Warm colors mean that the second experiment is less dense than KPP.

The realism of all eight simulated cross-sections in reproducing the baroclinic structure of the upper ocean is investigated by comparing the 29°W σ_2 cross-sections to one derived from the WOA 1994 climatology (Fig. 16). Experiment MIC has the largest rms difference from climatology (0.31, Table 5), but this is not much larger than the other experiments, which have differences ranging from 0.24 to 0.28. The dense mode water produced by experiment MIC is farther from climatology than the mode water produced by all experiments that included penetrating shortwave radiation (KPP, GISS, MY, PWP, and KTAIP). Also, the warm layer in the tropical Atlantic produced by experiment MIC is clearly too thin compared to climatology. In contrast,

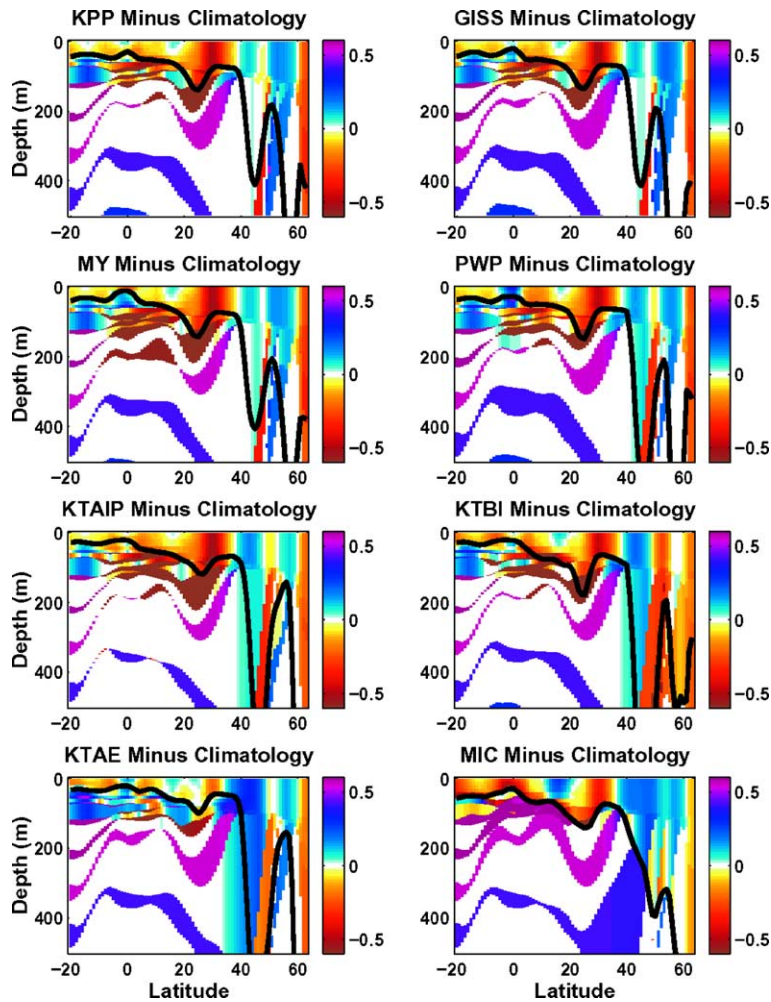


Fig. 16. Winter (mid-February) 29W cross-section of σ_2 difference between the eight primary experiments and WOA94 climatology. Differences result from changes in interface depth in the isopycnic coordinate interior, but become “continuous” near the surface. The MLB is represented by thick solid lines. Warm colors mean that the second experiment is less dense than climatology.

the warm layer produced by the hybrid experiments tends to be too thick, but is substantially closer to climatology than MIC. Part of this difference results from including shear instability mixing. Chen et al. (1994) noted that the KT mixed layer model typically provides insufficient vertical mixing in the tropical ocean, and included shear instability mixing from the PWP model into their KT model to reduce this problem. The present results support that decision. Numerical vertical diffusion produced by the hybrid grid generator also acts to thicken the tropical warm layer in hybrid coordinate simulations. Before the PLM algorithm and the reduction in minimum layer thickness below the p coordinate domain were implemented in the grid generator (Section 2.2), hybrid-coordinate simulations produced thicker warm layers than shown in Fig. 16, with the

thickness difference from climatology being about equal to and opposite in sign from the MIC difference.

The realism with which the baroclinic structure of the deeper ocean is reproduced is investigated by comparing 29°W σ_2 cross-sections over the upper 4000 m to a cross-section derived from the WOA 1994 climatology (Fig. 17). Very little difference is observed between the KPP and MIC experiments and climatology throughout the unventilated part of the water column. The other six hybrid experiments are not shown in Fig. 17 because they are almost identical to KPP. Rms differences for all eight experiments (Table 5) range from 0.12 for KPP and GISS to 0.15 for MIC. Since this climatology was used to initialize HYCOM, the interior ocean differences in Fig. 17 essentially represent the model drift that occurred over the >20 years of integration. The similarity in this drift for MIC and the hybrid experiments indicates that the hybrid grid generator is not causing significant problems as it acts to prevent slow drift away from the isopycnic reference density. The latter drift results from cabbeling (numerical and otherwise) due to horizontal advection/diffusion, vertical mixing, and vertical remapping of T and S by the grid generator. There is one aspect of the sections in Fig. 17 where experiment MIC performs better than KPP. All experiments produce water that is too light (warm) north of 40°N at depths between 2000 and 3000 m, but this bias is smallest in experiment MIC.

Since tropical Atlantic warm layer thickness differs substantially among experiments, the flow field may also differ substantially. Zonal velocity u is therefore examined in upper-ocean equatorial cross-sections (Fig. 18). Given the low-resolution of the experiments, core speeds for the Equatorial Undercurrent (EUC) are less than one-half of the magnitude observed in nature. The structure of this current in MIC differs substantially from the others, being thinner and residing about 20–30 m higher in the water column. The maximum magnitude of the EUC is sensitive to vertical mixing, ranging from about 0.25 m/s for experiment MY to over 0.35 m/s for experiment PWP and KTAE. The contribution of shear instability mixing below the mixed layer to the vertical structure of the zonal flow field is evident. In experiments KTAE and MIC where this process does not contribute to the mixing, a sharp boundary between the EUC and the westward South Equatorial Current tends to coincide with the mixed layer base. In the other experiments, the boundary between the SEC and EUC is not as sharp and tends to be displaced beneath the mixed layer.

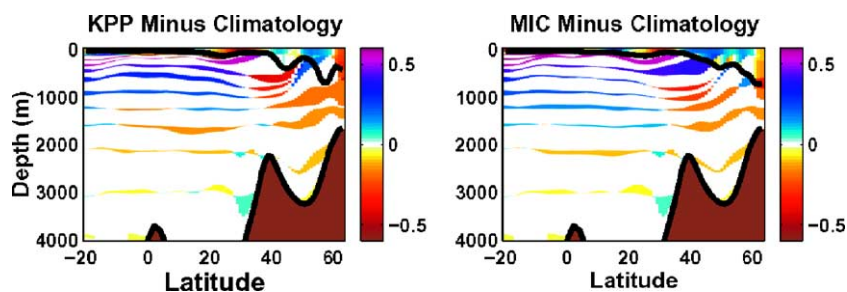


Fig. 17. Same as Fig. 16 for the upper 4000 m of the water column, but only for two of the eight primary experiments (KPP and MIC).

4.3.4. T, S versus ρ, S

To explore the impact of choosing T, S instead of ρ, S to be horizontally advected and diffused, and also vertically remapped by the hybrid grid generator, the KPP experiment (Table 1) is repeated using the ρ, S choice. Comparing winter surface temperature and 29°W cross-sections of σ_2 to climatology for these two KPP experiments (Fig. 19), it is evident that the choice of thermodynamical variables does not make a large difference in these simulated fields. The rms differences between the surface temperature fields and climatology are 0.90 (T, S) and 1.00 (ρ, S). The corresponding rms differences between the σ_2 cross-sections and climatology are 0.122 (T, S) and 0.145 (ρ, S). The model performance in these low-resolution climate simulations is slightly better when T, S is chosen. Conservation of T may therefore be slightly more important than avoiding numerically induced cabbeling.

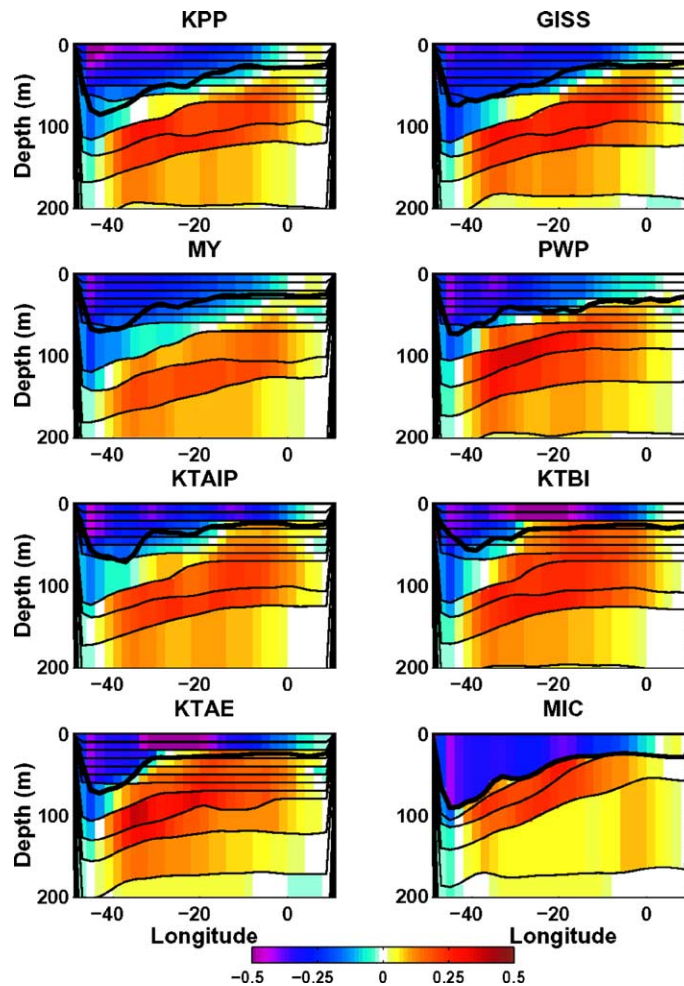


Fig. 18. Summer (mid-August) cross sections of zonal velocity (m/s) along the equator for the eight primary experiments.

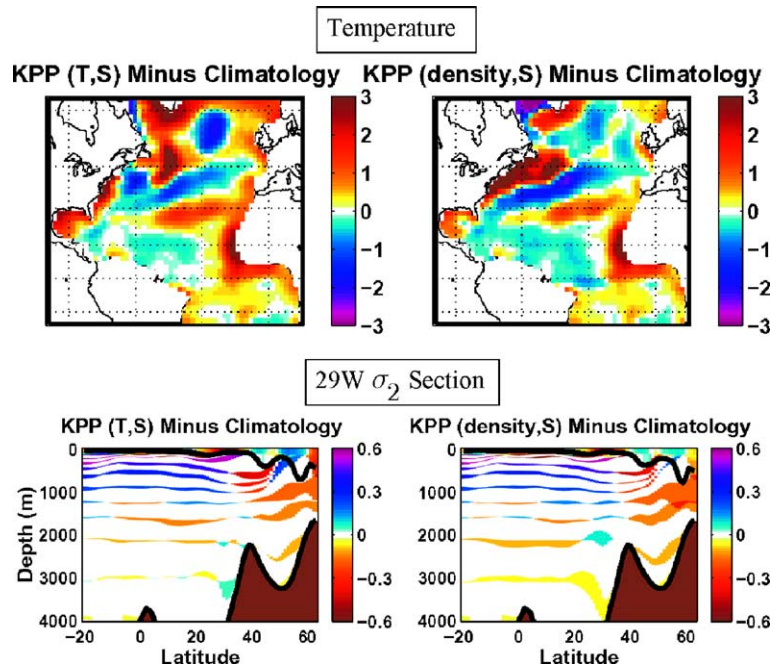


Fig. 19. Winter surface temperature difference maps (top) and 29°W σ_2 difference cross-sections (bottom), simulations minus climatology, for the standard KPP experiment where T , S (left) and ρ , S (right) are horizontally advected and diffused, and also remapped by the grid generator.

4.3.5. Penetrating shortwave radiation

The influence of shortwave radiation that penetrates beneath the KT mixed layer has been demonstrated here and in Rockford et al. (2001). To illustrate the influence of penetrating radiation on differential mixing models, experiments KPP, GISS, MY, and PWP were re-run with different choices of Jerlov water type. KPP experiments for water types 2 and 4 (Fig. 20) reveal that the depth to which shortwave radiation penetrates exerts a substantial influence on upper-ocean properties. Very similar difference patterns are obtained for the GISS, MY, and PWP models (not shown).

In general, winter and summer SST difference maps between water types 2 and 4 reveal that the summer (winter) hemisphere tends to be warmer (colder) as water type increases (as penetration depth is reduced). The winter σ_2 difference cross section along 29°W shows that the ocean is colder in the upper 200 m everywhere south of 40°N when penetration depth is reduced. This again confirms that the absence of penetrating shortwave radiation is partly responsible for the thin tropical Atlantic warm layer observed in MICOM (Section 4.3.3). Throughout the tropical Atlantic, the response to changing water type extends to depths beneath the direct influence of both the mixed layer and of the penetrating radiation, suggesting that subduction and advection play important roles. From the cross-section in Fig. 20, the subduction of colder water in the southern and central North Atlantic subtropical gyre may be a source of this water. In the subduction region, a thinner and warmer seasonal thermocline is produced during summer when penetration depth is reduced. The larger surface temperature increases heat flux out of the ocean

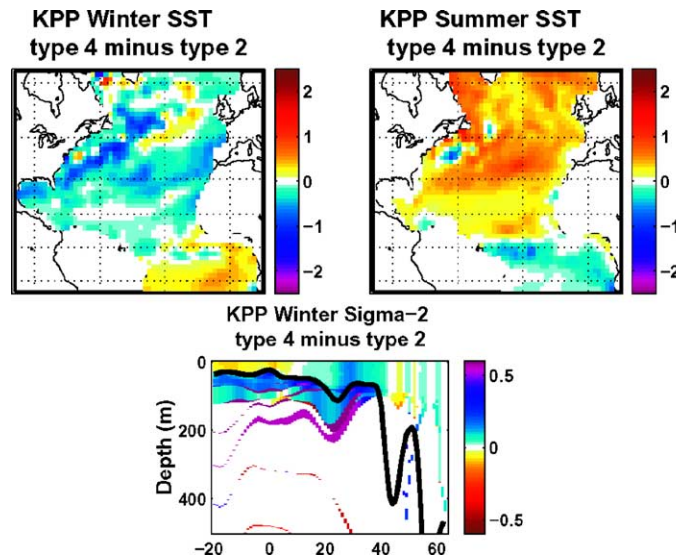


Fig. 20. Difference fields comparing KPP experiments using Jerlov water types of 2 and 4, with winter and summer SST at top and σ_2 along 29°W at the bottom. Difference patterns between types 2 and 3 are similar but smaller in magnitude, while difference patterns between types 2 and 5 are similar but larger in magnitude (not shown).

and thus reduces heat content over the upper 100–200 m in the subduction region. The net result is that colder water subducts during winter in the experiment with reduced penetration of shortwave radiation.

The substantial differences observed in Fig. 20 suggest that it is important to get the penetration correct in more realistic ocean simulations and in coupled ocean-atmosphere models since water clarity has substantial horizontal and temporal variability in nature. This can be accomplished by including an optical/biogeochemical model or by using satellite ocean color measurements to estimate penetration depths.

5. Discussion

HYCOM was developed to satisfy two primary criteria: (1) to create an ocean model with a flexible vertical coordinate system that is quasi-optimal in all oceanic regimes, and (2) to create an ocean model containing a suite of state-of-the-art vertical mixing algorithms. The multiple vertical mixing algorithms permit a user to determine to what extent scientific results are influenced or biased by the vertical mixing parameterization used, and also enables a user to choose the best mixing parameterization for the particular oceanic conditions that are being simulated.

HYCOM has undergone substantial additional development since Bleck (2002) demonstrated the feasibility of hybrid-coordinate ocean modelling. The present study focuses on recent HYCOM development, in particular the new vertical mixing algorithms that have been included (Table 1) and recent modifications to the hybrid grid generator. The three differential vertical mixing models (KPP, GISS and MY) permit vertical stratification to exist within the mixed layer.

Although this stratification is weak for model thermodynamical variables, the ageostrophic wind driven flow tends to form an Ekman spiral at the surface as expected with climatological forcing. The different mixing models can produce substantially different local behavior. Although these local differences do not produce large differences in the barotropic and surface baroclinic flow associated with the wind driven gyres, they do produce substantial large-scale differences in the thermohaline structure of the ocean.

All vertical mixing routines in HYCOM produce reasonable results. In general, HYCOM performance as evaluated by comparisons to climatology is best when the differential mixing models are used. Model performance is nearly as good when PWP mixing is employed. Unfortunately, the differences among fields using these four vertical mixing choices are a factor of 2–3 smaller than differences observed between simulated and climatological fields. As a result, it is impossible to statistically identify the best mixing scheme for low-resolution climatological simulations from the present analysis. Model performance tends to degrade slightly when the KT mixed layer is employed, but not enough to conclude that this model should never be used. In general, the worst model performance occurs when a KT mixed layer model is used without including shear instability mixing below the mixed layer and without allowing shortwave radiation to penetrate beneath the mixed layer. Since MICOM does not include these processes, the isopycnic coordinate (MICOM mode) experiment generally produced inferior results compared to the hybrid coordinate simulations using either the differential mixing models or the PWP model. The ability to include these processes in the hybrid coordinate framework is a clear benefit of HYCOM in comparison to MICOM. The negative impact of numerical diffusivity resulting from vertical coordinate relocation by the grid generator, and of other potential problems such as pressure gradient errors in sloping non-isopycnic coordinates, are smaller than the positive impact of converting from isopycnic to hybrid coordinates and including improved turbulence closure schemes.

Although differences among the different vertical mixing cases are small compared to differences between simulations and climatology, they are still large enough to be significant. This is especially true for SST and surface heat flux fields, where rms differences between simulations using different mixing schemes typically equal 0.33–1.14 °C and 20–48 W/m², respectively. Changing the vertical mixing scheme may therefore significantly alter the storage and flux of heat in the simulated ocean and thus produce significant changes in climate produced by a coupled climate model.

Biases and errors present in these HYCOM simulations should be substantially reduced in high-resolution simulations that are driven by more-accurate forcing that resolves synoptic and diurnal variability. Such simulations will provide a much more stringent test of the performance of HYCOM vertical mixing schemes. Work is therefore underway to evaluate HYCOM in a wide range of environmental conditions, including the coastal ocean and the ocean response to hurricanes.

Acknowledgements

Development of HYCOM commenced with National Science Foundation support under grant number OCE9415911. Present support is provided through the Office of Naval Research through

grant number N00014-99-1-1066 (under the National Oceanographic Partnership) and also through grant number N00014-99-1-0048. ONR This analysis benefited from discussions with E. Chassignet, R. Bleck, and L. Smith. A. Howard and V. Canuto of GISS provided the one-dimensional code for inclusion in HYCOM.

References

- Bleck, R., 1998. Ocean modelling in isopycnic coordinates. In: Chassignet, E.P., Verron, J. (Eds.), *Ocean Modelling and Parameterization*. In: NATO Science Series C: Mathematical and Physical Sciences, 516. Kluwer Academic Publishers, Dordrecht, pp. 4223–4448 (Chapter 18).
- Bleck, R., 2002. An oceanic general circulation model framed in hybrid isopycnic—Cartesian coordinates. *Ocean Model.* 4, 55–88.
- Bleck, R., Benjamin, S., 1993. Regional weather prediction with a model combining terrain-following and isentropic coordinates, part 1: model description. *Mon. Wea. Rev.* 121, 1770–1785.
- Bleck, R., Hanson, H.P., Hu, D., Kraus, E.B., 1989. Mixed layer–thermocline interaction in a three-dimensional isopycnic coordinate model. *J. Phys. Oceanogr.* 19, 1417–1439.
- Bleck, R., Rooth, C., Hu, D., Smith, L.T., 1992. Ventilation patterns and mode water formation in a wind- and thermodynamically driven isopycnic coordinate model of the North Atlantic. *J. Phys. Oceanogr.* 22, 1486–1505.
- Bleck, R., Halliwell, Jr., G.R., Wallcraft, A.J., Carroll, S., Kelly, K., Rushing, K., 2002. Hybrid coordinate ocean model (HYCOM) user's manual: details of the numerical code. Available from <<http://hycom.rsmas.miami.edu>>.
- Brydon, D., Sun, S., Bleck, R., 1999. A new approximation of the equation of state for sea water, suitable for numerical ocean models. *J. Geophys. Res.* 104, 1537–1540.
- Canuto, V.M., Howard, A., Cheng, Y., Dubovikov, M.S., 2001. Ocean turbulence. Part I: one-point closure model. Momentum and heat vertical diffusivities. *J. Phys. Oceanogr.* 31, 1413–1426.
- Canuto, V.M., Howard, A., Cheng, Y., Dubovikov, M.S., 2002. Ocean turbulence. Part II: vertical diffusivities of momentum, heat, salt, mass, and passive scalars. *J. Phys. Oceanogr.* 32, 240–264.
- Chassignet, E.P., Smith, L.T., Bleck, R., Bryan, F.O., 1996. A model comparison: numerical simulations of the North and Equatorial Atlantic oceanic circulation in depth and isopycnic coordinates. *J. Phys. Oceanogr.* 26, 1849–1867.
- Chassignet, E.P., Arango, H., Dietrich, D., Ezer, T., Ghil, M., Haidvogel, D.B., Ma, C.-C., Mehra, A., Paiva, A.M., Sirkes, Z., 2000. DAMEE-NAB: the base experiments. *Dyn. Atmos. Oceans* 32, 155–184.
- Chassignet, E.P., Smith, L.T., Halliwell Jr., G.R., Bleck, R., 2003. North Atlantic simulations with the hybrid coordinate ocean model (HYCOM): impact of the vertical coordinate choice, reference density, and hermobaricity. *J. Phys. Oceanogr.* 34, 2504–2526.
- Chen, D.L., Rothstein, M., Busalacchi, A.J., 1994. A hybrid vertical mixing scheme and its application to tropical ocean models. *J. Phys. Oceanogr.* 24, 2156–2179.
- Gaspar, P., 1988. Modelling the seasonal cycle of the upper ocean. *J. Phys. Oceanogr.* 18, 161–180.
- Halliwell, Jr., G.R., 1997. Simulation of decadal/interdecadal variability the North Atlantic driven by the anomalous wind field. In: *Proceedings, Seventh Conference on Climate Variations, Long Beach, CA*, pp. 97–102.
- Halliwell Jr., G.R., 1998. Simulation of North Atlantic decadal/multi-decadal winter SST anomalies driven by basin-scale atmospheric circulation anomalies. *J. Phys. Oceanogr.* 28, 5–21.
- Hu, D., 1996. On the sensitivity of thermocline depth and meridional heat transport to vertical diffusivity in OGCMs. *J. Phys. Oceanogr.* 26, 1480–1494.
- Hu, D., 1997. Global-scale water masses, meridional circulation, and heat transport simulated with a global isopycnic ocean model. *J. Phys. Oceanogr.* 27, 96–120.
- Jerlov, N.G., 1976. *Marine Optics*. Elsevier, New York.
- Kara, A.B., Rochford, P.A., Hurlburt, H.E., 2000a. An optimal definition for ocean mixed layer depth. *J. Geophys. Res.* 105, 16803–16821.
- Kara, A.B., Rochford, P.A., Hurlburt, H.E., 2000b. Efficient and accurate bulk parameterizations of air-sea fluxes for use in general circulation models. *J. Atmos. Ocean Tech.* 17, 1421–1438.

- Large, W.G., McWilliams, J.C., Doney, S.C., 1994. Oceanic vertical mixing: a review and a model with a nonlocal boundary layer parameterization. *Rev. Geophys.* 32, 363–403.
- Large, W.G., Danabasoglu, G., Doney, S.C., Mc Williams, J.C., 1997. Sensitivity to surface forcing and boundary layer mixing in a global ocean model: annual-mean climatology. *J. Phys. Oceanogr.* 27, 2418–2447.
- Levitus, S., Boyer, T., 1994. In: *World Ocean Atlas 1994 Volume 4: Temperature*. NOAA Atlas NESDIS 4. US Department of Commerce, Washington, DC.
- Levitus, S., Burgett, R., Boyer, T., 1994. In: *World Ocean Atlas 1994 Volume 3: Salinity*. NOAA Atlas NESDIS 3. US Department of Commerce, Washington, DC.
- McDougall, T.J., Dewar, W.K., 1998. Vertical mixing and cabbeling in layered models. *J. Phys. Oceanogr.* 28, 1458–1480.
- Mellor, G.L., 1998. Users manual for a three-dimensional, primitive equation numerical ocean model. Available on the Princeton Ocean Model web site.
- Mellor, G.L., Yamada, T., 1982. Development of a turbulence closure model for geophysical fluid problems. *Rev. Geophys. Space Phys.* 20, 851–875.
- Murphy, A.H., 1988. Skill scores based on the mean square error and their relationships to the correlation coefficient. *Mon. Wea. Rev.* 116, 2417–2424.
- New, A., Bleck, R., 1995. An isopycnic model of the North Atlantic, part II: interdecadal variability of the subtropical gyre. *J. Phys. Oceanogr.* 25, 2700–2714.
- New, A., Bleck, R., Jia, Y., Marsh, R., Huddleston, M., Barnard, S., 1995. An isopycnic model of the North Atlantic, part I: model experiments. *J. Phys. Oceanogr.* 25, 2667–2699.
- Niiler, P.P., Kraus, E.B., 1977. One-dimensional models of the upper ocean. In: Kraus, E.B. (Ed.), *Modelling and Prediction of the Upper Layers of the Ocean*. Pergamon, New York, pp. 143–172.
- Paiva, A.M., Chassignet, E.P., Mariano, A.J., in press. Numerical simulations of the North Atlantic subtropical gyre: sensitivity to boundary conditions and horizontal resolution, *Deep-Sea Res.*
- Price, J.F., Weller, R.A., Pinkel, R., 1986. Diurnal cycling: observations and models of the upper ocean response to diurnal heating, cooling, and wind mixing. *J. Geophys. Res.* 91, 8411–8427.
- Roberts, M.J., Marsh, R., New, A.L., Wood, R.A., 1996. An intercomparison of a Bryan–Cox-type ocean model and an isopycnic ocean model, part I: the subpolar gyre and high-latitude processes. *J. Phys. Oceanogr.* 26, 1495–1527.
- Rockford, P.A., Kara, A.B., Wallcraft, A.J., Arnone, R.A., 2001. Importance of solar subsurface heating in ocean general circulation models. *J. Geophys. Res.* 106, 30923–30938.
- Sun, S., Bleck, R., Rooth, C., Dukowicz, J., Chassignet, E., Killworth, P., 1999. Inclusion of thermobaricity in isopycnic-coordinate ocean models. *J. Phys. Oceanogr.* 29, 2719–2729.
- Turner, J.S., Kraus, E.B., 1967. A one-dimensional model of the seasonal thermocline II: the general theory and its consequences. *Tellus* 19, 98–105.
- Willebrand, J., Barnier, B., Boning, C.W., Dieterich, C., Killworth, P.D., LeProvost, C., Jia, Y., Molines, J.M., New, A.L., 2001. Circulation characteristics in three eddy-permitting models of the North Atlantic. *Prog. Oceanogr.* 48, 123–161.